NAVAL POSTGRADUATE SCHOOL
Monterey, California

THESIS

ARCTIC CYCLONES
AND
MARGINAL ICE ZONE (MIZ) VARIABILITY

by

Steven John Rutherford

March, 1993

Thesis Advisor: Kenneth L. Davidson
Second Reader: Wendell A. Nuss

REPORT DOCUMENTATION PAGE

Form Approved
OMB No. 0704-0188

1. AGENCY USE ONLY (Leave blank)	2. REPORT DATE	3. REPORT TYPE AND DATES COVERED
	March, 1993	Master's Thesis

4. TITLE AND SUBTITLE
ARCTIC CYCLONES AND MARGINAL ICE ZONE (MIZ) VARIABILITY

5. FUNDING NUMBERS

6. AUTHOR(S)
LT Steven John Rutherford, USN

7. PERFORMING ORGANIZATION NAME(S) AND ADDRESS(ES)
Naval Postgraduate School
Monterey, CA 93943-5000

8. PERFORMING ORGANIZATION REPORT NUMBER

9. SPONSORING/MONITORING AGENCY NAME(S) AND ADDRESS(ES)
Naval Postgraduate School
Monterey, CA 93943-5000

10. SPONSORING/MONITORING AGENCY REPORT NUMBER

11. SUPPLEMENTARY NOTES
The views expressed in this thesis are those of the author and do not reflect the official policy or position of the Department of Defense or the U.S. Government.

12a. DISTRIBUTION/AVAILABILITY STATEMENT
Unlimited

12b. DISTRIBUTION CODE

13. ABSTRACT *(Maximum 200 words)*

The Seasonal Ice Zone Experiment (SIZEX), conducted in January 1992, was designed as the European Space Agency's ERS-1 synthetic-aperature radar (SAR) validation experiment. The satellite was placed in a three day exact repeat orbit, with ascending and descending passes which crossed the Greenland Sea marginal ice zone. In conjunction with SAR imagery collected by the Nansen Environmental and Remote Sensing Center, the research vessel Hakon Mosby recorded meteorological data on station near the ice edge. The marginal ice zone was subjected to atmospheric and oceanographic forcing during the 7-16 January period which resulted in significant changes in ice edge morphology. As intense low pressure systems propagated across the Greenland Sea, strong easterly and northerly winds dominated oceanographic forcing and created a compact ice edge which correlated with the 50% ice concentration isopleth from the SSM/I passive microwave sensor. Conversely, during periods of weak atmospheric forcing, the ice edge became diffuse and the ice edge morphology was determined by a variety of oceanic circulations. In this instance the actual ice edge position was well correlated with a 30% concentration isopleth.

14. SUBJECT TERMS	15. NUMBER OF PAGES
arctic cyclones, marginal ice zone, morphology, SIZEX, ERS-1, SAR, backscatter	90
	16. PRICE CODE

17. SECURITY CLASSIFICATION OF REPORT	18. SECURITY CLASSIFICATION OF THIS PAGE	19. SECURITY CLASSIFICATION OF ABSTRACT	20. LIMITATION OF ABSTRACT
Unclassified	Unclassified	Unclassified	Unlimited

Approved for public release; distribution is unlimited.

Arctic Cyclones and Marginal Ice Zone (MIZ) Variability

by

Steven John Rutherford
Lieutenant, United States Navy
B.S., State University of New York at Albany, 1984

Submitted in partial fulfillment of the
requirements for the degree of

MASTER OF SCIENCE IN METEOROLOGY
AND PHYSICAL OCEANOGRAPHY

from the

NAVAL POSTGRADUATE SCHOOL
March 1993

Author: _____
Steven John Rutherford

Approved by: _____
Kenneth L. Davidson, Thesis Advisor

_____
Wendell A. Nuss, Second Reader

_____
Robert L. Haney, Chairman,
Department of Meteorology

ABSTRACT

The Seasonal Ice Zone Experiment (SIZEX), conducted in January 1992, was designed as the European Space Agency's ERS-1 synthetic-aperature radar (SAR) validation experiment. The satellite was placed in a three-day exact repeat orbit, with ascending and descending passes which crossed the Greenland Sea marginal ice zone. In conjunction with SAR imagery collected by the Nansen Environmental and Remote Sensing Center, the research vessel HÄKON MOSBY recorded meteorological data on station near the ice edge in the Greenland Sea. The marginal ice zone was subjected to atmospheric and oceanographic forcing during the 7–16 January period which resulted in significant changes in ice edge morphology. As intense low-pressure systems propagated across the Greenland Sea, strong easterly and northerly winds dominated oceanic forcing and created a compact ice edge which correlated with the 50% ice concentration isopleth from the SSM/I passive microwave sensor. Conversely, during periods of weak atmospheric forcing, the ice edge became diffuse and the ice edge morphology was determined by a variety of oceanographic circulations. In such instances, the actual ice edge position was well correlated with the SSM/I 30% ice concentration isopleth.

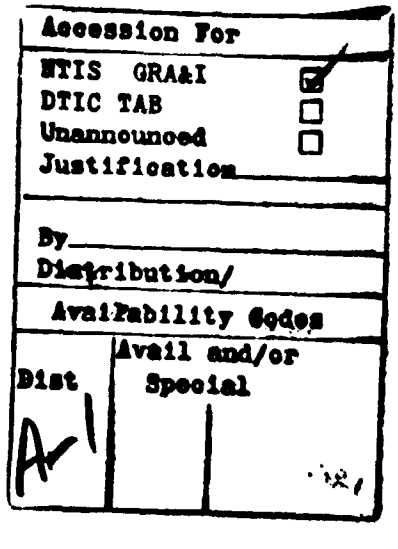

TABLE OF CONTENTS

LIST OF FIGURES

ACKNOWLEDGMENTS

The author would like to extend his most sincere thanks for the support, guidance, and patience provided by Professors Kenneth L. Davidson and Wendell A. Nuss in the conduct of the research and preparation of this thesis. The Nansen Environmental and Remote Sensing Center (NERSC) in Solheimsvik, Norway was also a source of invaluable support and feedback during the research and thesis preparation. NERSC's Stein Sandven, Ola Johannessen, Johnny Johannessen, and Kjell Kloster dedicated their time and resources to assist in the interpretation of SAR imagery. For their gracious efforts, I extend my thanks and admiration. The Naval Postgraduate School's Boundary Layer Group, particularly Peter Guest, Tamara Neta, and Paul Frederickson, provided sound advice and assistance in the preparation of this thesis, which were also greatly appreciated. NPS participation in SIZEX '92 was funded by the Oceanographer of the Navy (OP-096), via NOARL-SSC, and the NPS Direct Research Funding Program. Finally, I would like to thank my wife for her infinite patience, support, and love throughout my graduate education. I could not have completed this research or graduated from this institution without her by my side.

I. INTRODUCTION AND BACKGROUND

A. PURPOSE

The marginal ice zone (MIZ), the interface between arctic pack ice and open ocean, is a dynamic region which is influenced by the development and translation of high latitude cyclones and anticyclones in the vicinity of the ice edge. Conversely, over large regions, seasonal and short term shifts in the position of the MIZ act to modulate the occurrence of cyclonic activity on a synoptic time scale (Barry, 1986). The MIZ air-ice-sea processes and exchanges determine the advance and retreat of sea ice, influence global climate, impact marine productivity and effect naval operations (Johannessen et al., 1984). As the physical characteristics of the MIZ change due to convergent or divergent motion associated with the atmospheric and oceanic circulation, the atmospheric boundary layer (ABL) and its effective drag coefficients are modified. Thorndike and Colony (1982) have noted that the principle predictor of ice motion is the wind.

Overland (1985) and Overland and Davidson (1992) concluded that the drag coefficient is dependent upon the surface roughness and ABL stability. Because the drag coefficient relates the surface stress on the ice to the wind speed, it is considered a critical parameter in modeling regional ice motion. This atmosphere-ice-ocean interaction remains poorly understood to date.

With the advent of synthetic-aperture radar (SAR) researchers now have an unprecedented opportunity to obtain high resolution imagery of sea ice unencumbered by cloud cover or darkness. Ice type classification, concentration and drag coefficient determinations are now possible through remote sensing.

Ultimately this should improve our understanding of air-ice-sea interaction processes.

B. OBJECTIVES

The primary goal of this research was to evaluate the effects of a synoptic disturbance's strong winds and the associated wind shifts upon the MIZ morphology. Past studies have documented a relationship between the interannual sea ice extent and atmospheric circulation patterns (Johnson, 1980). Short term sea ice variations have been related to individual synoptic events (Carleton, 1984 and Campbell et al., 1987) using microwave radiometer-derived surface brightness temperatures. A significant drawback to these studies was the poor resolution (effective pixel resolution of 30 square km) associated with the sensor. Johannessen (1993) introduced a SAR conceptual model which related commonly observed ice edge features to specific atmospheric and/or oceanic forcing. An extensive literature search has failed to find studies relate short term variations of the MIZ to individual cyclones or anticyclones using high resolution SAR imagery.

The second goal of the study was to characterize the nature of the cyclones which act to modify the morphology of the ice edge in an effort to better understand the dynamics of the atmosphere-sea ice-ocean relationship. The low pressure systems which propagated over the Greenland Sea were described in terms of their residence time, intensity and speed of advance.

Finally, the East Greenland Sea ice edge position determined from the interpretation of ERS-1 SAR imagery was compared to the ice edge position inferred from ice concentration isopleths obtained from the Defense Meteorological Satellite Program's (DMSP) operational Special Sensor Microwave Instrument (SSM/I).

C. FORMAT

Chapter I describes the goals and objectives of the Seasonal Ice Zone Experiment (SIZEX) 1992. This research was based upon the data collected during this experiment. Chapter I also summarizes related research in arctic and marginal ice zone processes in an effort to provide the reader with an appreciation of the complexity of MIZ air-ice-ocean interactions.

Chapter II describes the various data sources for SIZEX 92 and their analyses. A detailed account of a) the meteorology during the experiment; b) observed changes in the MIZ morphology; and c) SSM/I ice concentration isopleths versus SAR ice edge positions, are provided.

Chapter III summarizes the results and conclusions obtained during the course of this research. Recommendations for future research efforts are also included in this chapter.

Lastly, all figures referenced in a particular chapter may be found at the end of the section where they were referenced.

D. BACKGROUND

Related studies were reviewed that concerned ice morphology and arctic air-sea interaction. A brief description of the goals and data collection objectives for SIZEX 1992 are presented below. The ocean surface circulation, physical processes in the MIZ and climatology of the Greenland and Barents Seas were reviewed to gain a better understanding of the environment.

SIZEX '92, a post-launched ERS-1 field experiment, was conducted between January and March 1992 in the Greenland and Barents Seas. The experiment was divided into two segments, designated as SIZEX I and SIZEX II. SIZEX I was augmented with real time SAR, DMSP SSM/I and NOAA AVHRR

data. SIZEX II was conducted with the same suite of satellite sensors. Routine SAR imagery was terminated after 24 March.

SIZEX I was conducted in the Greenland Sea between January 3-26. The oceanography objectives focused primarily on the investigation of chimneys in the Boreas Basin and Greenland Basin. Water masses were sampled and the velocity structure was determined in each basin. The sampling objectives were to identify deep or intermediate water masses which had been elevated to the surface by preconditioning. ERS-1 validation objectives included the distinction between open water and thin ice by SAR, the distinction among thin ice types and validation of wind fronts and upper ocean circulation features outside the ice edge as observed by SAR.

SIZEX II was conducted in the Barents Sea between February 24 and March 25. Its objectives for ERS-1 validation included SAR sea ice classification and a SAR ice motion algorithm. Additional objectives involved ice edge processes such as eddies, jets and vortex pairs, and ambient noise measurements with respect to ice interaction.

The overall objective of SIZEX '92 was to estimate and validate ice parameters such as ice kinematics, ice concentration and ice type classification derived from ERS-1 SAR. Ultimately real time estimates of these parameters will be used in conjunction with atmospheric and oceanographic variables as input to coupled air-ice-ocean models. This research dealt exclusively with data obtained during SIZEX I.

1. Results of Past Field Experiments

A series of field experiments have been conducted in the eastern and western arctic in order to study the air-ice-ocean interactions that influence the local and hemispheric weather and climate. In 1984, the Marginal Ice Zone Experiment (MIZEX) field program was conducted in the East Greenland Sea

using the scanning multichannel microwave radiometer (SMMR) and five microwave (active and passive) remote sensing aircraft. The active and passive microwave data obtained by the aircraft provided a comprehensive sequential description of the mesoscale sea ice morphology of the Fram Strait MIZ and its variations (Campbell et al., 1987). Figure 1 shows a series of sea ice concentration maps depicting both the sea ice extent and concentration for the period of June 8-30 1984. The ice concentration isopleths were computed using a SMMR ice algorithm. The large footprint associated with the SMMR sensor combined with the sharpness of the ice edge made it impossible to definitively identify the position of the ice edge. However a comparison of the SMMR-derived ice concentrations with high resolution aircraft observations showed that for diffuse ice edges the 30% SMMR isopleth closely approximated the observed ice edge position. Similarly, the 40-50% SMMR isopleths were well-correlated with the compact ice edge.

Within the MIZ, ice morphology is dependent upon the combined effects of atmospheric and oceanic forcing. One might anticipate that ice edge characteristics are at least partially dependent on the direction and magnitude of the wind. In turn, the surface stress imparted to the ice edge is a function of the surface roughness. To complicate matters further, the respective contributions of either mechanism vary from day to day and region to region. For instance, in the vicinity of the East Greenland Current one may expect the regional-scale oceanography to dominate atmospheric forcing in the absence of a strong synoptic circulation.

Figure 2 from Campbell et al. (1987) shows the importance of the atmosphere's role in changing MIZ morphology. In general, observations indicate that strong winds tend to smooth MIZ morphology, regardless of wind direction. At first this may appear contrary to reason. However, wind-generated shear in

the ice pack, internal ice stress and melting across the polar front may act to smooth ice edge irregularities.

The wind-driven ice transport generally contains a component along the ice edge. Results obtained by Shuchman et al. (1987) show that strong shear occurs in the MIZ during strong wind events. Wind-driven ice transport normal to the ice edge also tends to smooth large scale regions of the MIZ. For instance, internal stresses produced by on-ice transport act to remove large-scale irregularities or protuberances in the ice edge. Off-ice transport is subject to rapid melting as the ice drifts across the polar front into warm north Atlantic water. Hence, the north Atlantic water acts as a barrier that restricts southward ice transport (Campbell et al., 1987), yielding a more uniform ice edge that reflects the horizontal temperature distribution in the region.

MIZEX '84 results also indicate that strong on-ice winds produced pronounced variations in sea ice concentration gradients (the percent change in ice concentration divided by the distance over which the change occurs). Off-ice winds tended to relax the ice concentration gradient. Ice divergence, in the absence of strong currents, results from a greater aerodynamic roughness and bulk drag coefficient in the ice edge region than in the interior (Guest and Davidson, 1987).

The areal distribution and variable intensity values in SAR image data are impacted by the same ice field characteristics (ice concentration, surface roughness and floe size) that are responsible for variations in the drag coefficient. Burns and Kellner (1988) conducted a study to determine the relationship between these characteristics as derived from SAR and the drag coefficient in the MIZ. Formulation of an effective drag coefficient in terms of ice concentration, floe edge height, floe radius and roughness was devised which qualitatively agreed with field observations, although it overestimated the drag in

very rough areas. Nevertheless, this was an important step in utilizing SAR data to estimate air-sea-ice interactions along the MIZ.

The first extensive SAR data collection in the Barents Sea was conducted during SIZEX '89. An important part of the study was the analysis of four SAR mosaics from the area between Bjornoya and Hopen. These mosaics showed a complex and highly variable ice edge structure, consisting of ice bands, ice tongues, eddies, open bights as well as unquantifiable features. The images demonstrated quite clearly that our understanding of ice edge dynamics was incomplete and that further research was required.

2. Ocean Surface Circulation and Physical Processes in the MIZ

a. Circulation

It is readily apparent from Figure 2 that strong winds play an important role in affecting ice edge morphology. However it is equally clear that another mechanism is responsible for significant changes in ice edge character when atmospheric forcing is weak. This mechanism must be the ocean surface circulation.

Surface circulation forcing of the ice edge remains uncertain. Aagaard (1970) suggested that the wind stress within these regions is sufficiently strong to account for the observed circulations. Worthington (1970) maintained that thermohaline processes were the dominant forcing mechanism, while Mosby (1962) proposed that the inflowing Atlantic water through the Faeroe-Shetland Channel and outflowing water via the East Greenland Current forced the circulation pattern.

(1) Greenland Sea. The bottom topography strongly influences the circulation and distribution of the water masses (Johannessen, 1986). Comparison of the bathymetry and circulation, Figures 3 and 4, suggests that the East Greenland Current's eastern boundary is correlated with Greenland's

continental slope. Much of the inflow into the Greenland (and Barents) Sea is through the Faeroe-Shetland Channel. There, the current follows the Norwegian coast and a portion branches off into the Barents Sea. Another part follows the continental slope northward towards Spitzbergen. As the surface water flows northward, it follows one of two pathways. It either converges with the East Spitzbergen Current, sinks and flows into the Arctic Ocean along the western edge of Spitzbergen, or it branches westward into the East Greenland Current. Hence, the circulation in the Greenland Sea takes the form of a large cyclonic gyre.

(2) Barents Sea. The Norwegian Coastal Current and Norwegian Atlantic Current (Figure 4) are the major inflows into the Barents Sea. Part of the Norwegian Atlantic water penetrates directly into the Barents Sea while another part closely parallels the Norwegian coast as the Norwegian Coastal Current. Surface outflow occurs via the East Spitzbergen Current and Bear Island Current.

b. Physical Processes in the MIZ

(1) Wave-Induced Breakup. As open ocean waves and swell impinge upon the ice comprising the MIZ, a stress is placed on the floes, inducing the ice to bend. If the stress is too large, the ice will break. If the northerly wind stress component advects large areas of continuous ice sheet toward the ice margin, open ocean waves can propagate through the sheet and induce breakup in areas of structural weakness. Only the longest period swell propagates more than a few kilometers into the ice. Thus wave-induced breakup is most prominent in ice margins exposed to a long fetch of stormy sea (Wadhams, 1986).

As a first order approximation, one might conclude that the ice field is characterized by a distribution of floe sizes with distance from the ice edge. The local wave field at the ice edge would produce small floes. Ice slightly

farther from the margin would be partially protected, as the floes seaward damp the wave field. Hence, larger floes would not be susceptible to breakup. In this manner, average floe size should increase with distance from the ice margin. However, observations do not support this hypothesis. Rather, floes are more mobile, have greater drag coefficients (due to rafting and numerous collisions which produce deformation), and thus respond to the wind field. Wind may advect large floes toward the ice margin, where they are subjected to the local wave field. Additionally, ocean eddies along the ice edge are responsible for the transport of ice floes toward the ice margin.

(2) Mass Transfer Associated with Eddies. The formation of large amplitude meanders along the ice edge may indicate the presence of eddies. A eddy can cause a loss of mass (in the form of ice floes) from the MIZ by drawing ice toward the margin, where it either melts or disintegrates due to wave action. These features are prevalent along the MIZ and can dominate ice morphology in the absence of strong synoptic forcing.

(3) Lateral and Wave-Induced Melting. In addition to wave-induced breakup, floes are advected by the wind field, producing regions of ice drift divergence and open water leads. In such instances the heat transfer mechanism for lateral melting is particularly efficient. If conditions are calm, the absorption of solar radiation (summer months) is concentrated in the upper one or two meters of the ocean. If conditions are not calm, turbulence and wind-wave motion around the floe periphery increase the melt rate (Wadhams, 1986). Furthermore, water can penetrate into structurally weak portion of the floe, thus accelerating its breakup.

3. Greenland and Barents Seas Climatology

High latitude weather is closely tied to the location of the circumpolar vortex, which describes the southern extent of the polar air masses into middle

latitudes. The circumpolar vortex is the term given to the concentric pattern of height contours centered about the pole. Regions of increased horizontal height gradients correspond to zones of enhanced baroclinicity, along which fronts and cyclones form. Figure 5 shows the January circumpolar vortex. Note the tight spacing between the contours in winter months, implying a greater frequency and intensity of cyclonic activity.

The winter (December-February) cyclone pattern depicted in Figure 6 from Serreze and Barry (1988) shows high frequencies[1] between Spitzbergen and Scandinavia and a separate area over the eastern Barents Sea. Serreze and Barry (1988) suggest that there are significant regional differences in mean cyclone pressures. Particularly, winter cyclones in the Barents and Greenland Seas are much deeper than those formed in other regions. This tendency may be attributed to a variety of factors. In passing over mostly ocean surfaces, the cyclones may degrade more slowly from frictional effects than cyclones entering from land surfaces (LeDrew, 1984). It is also likely that latent heat fluxes and pronounced sea surface temperature gradients play an important role. One descriptive parameter is the cyclone constancy, which is a measure of the persistence in the direction of motion. That is, a high percentage implies that cyclones within a region travel in much the same direction. The Barents and Greenland Seas are characterized by high constancy relative to other regions.

[1]Low pressure system totals in an equal area grid box were converted into percent frequencies. Only systems that appeared on at least two consecutive daily charts are included.

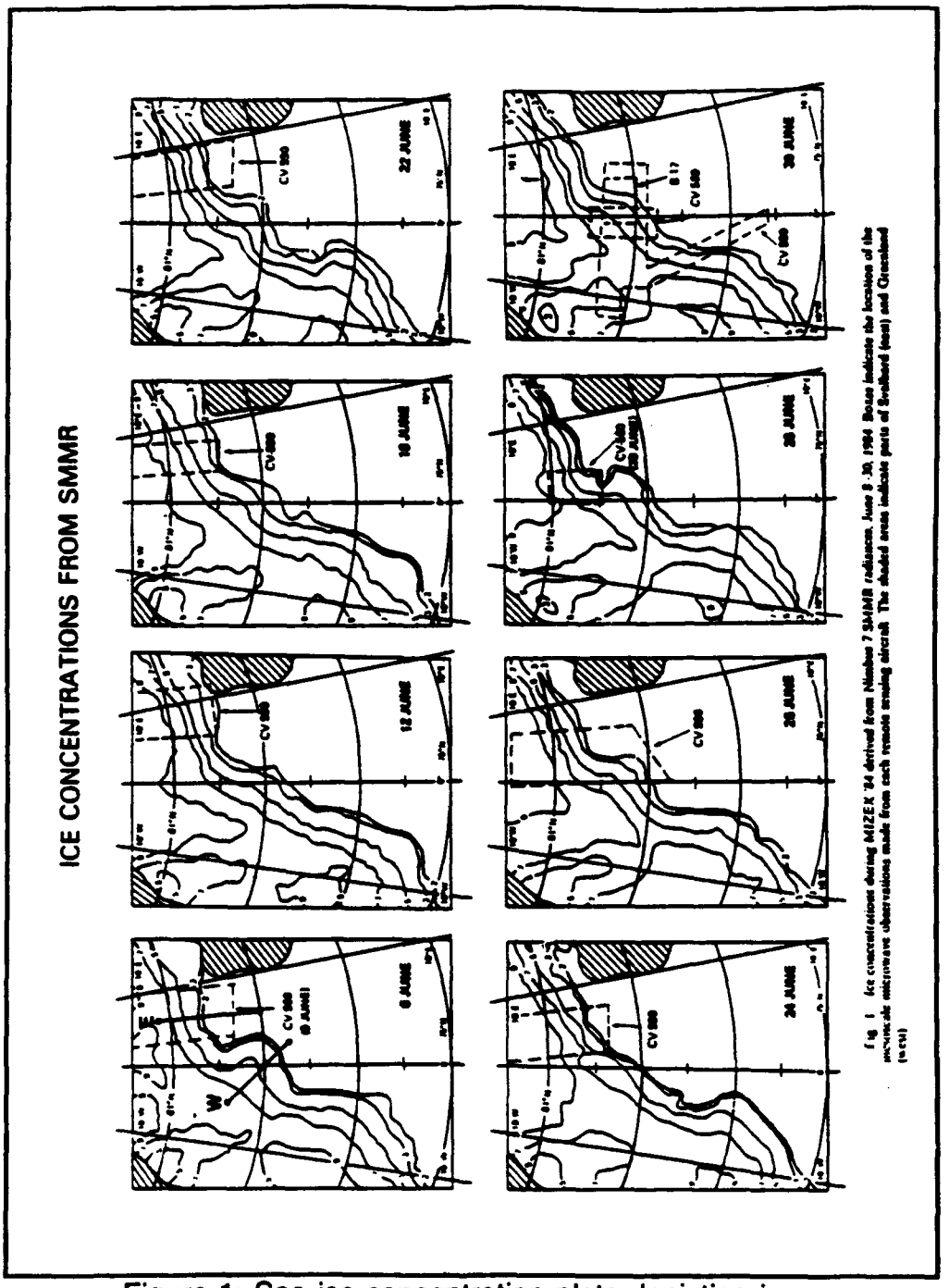

Figure 1: Sea ice concentration plots depicting ice extent and concentration (from Campbell et al, 1987)

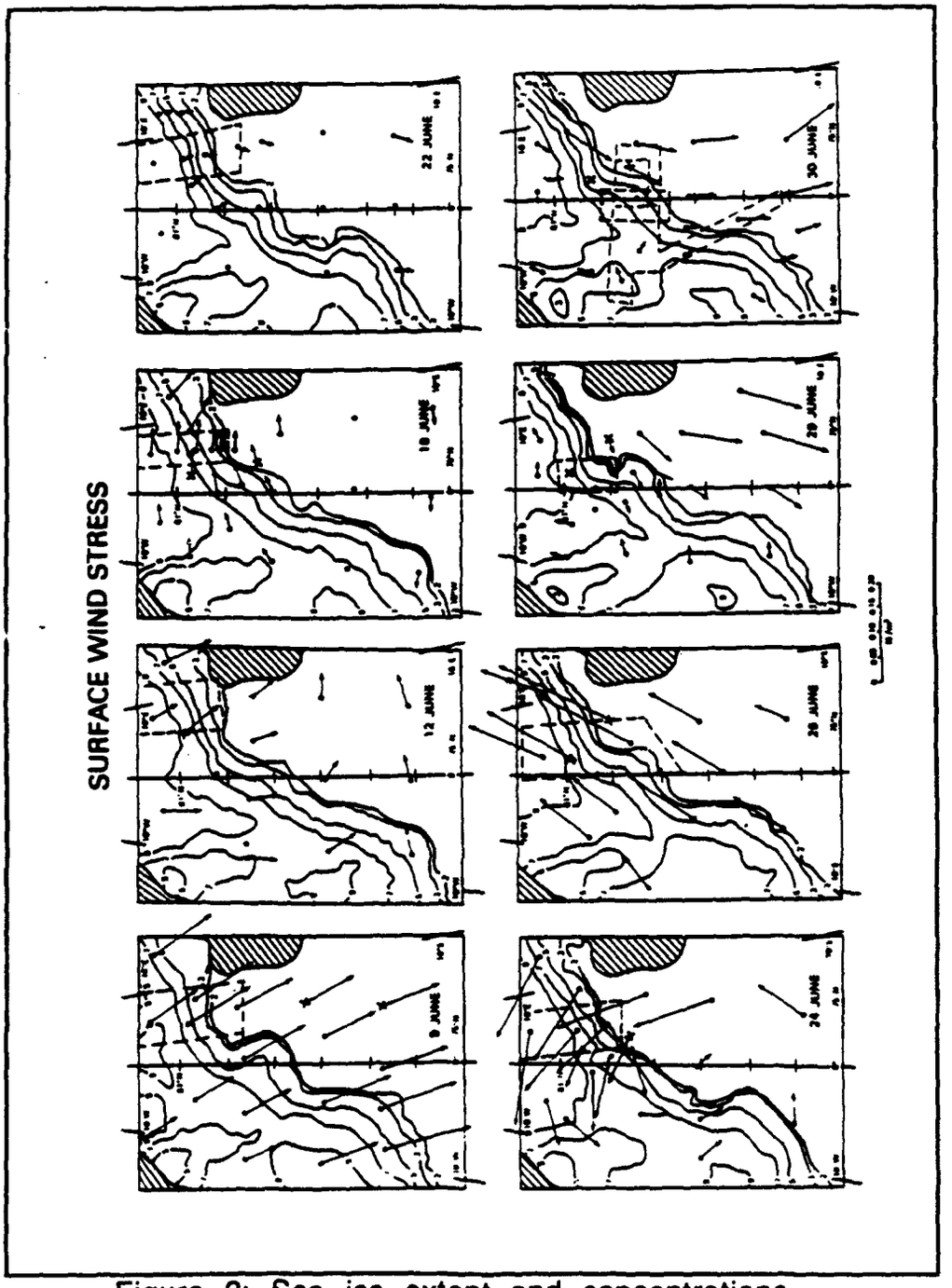

Figure 2: Sea ice extent and concentrations. Arrows represent wind stress (from Campbell et al, 1987)

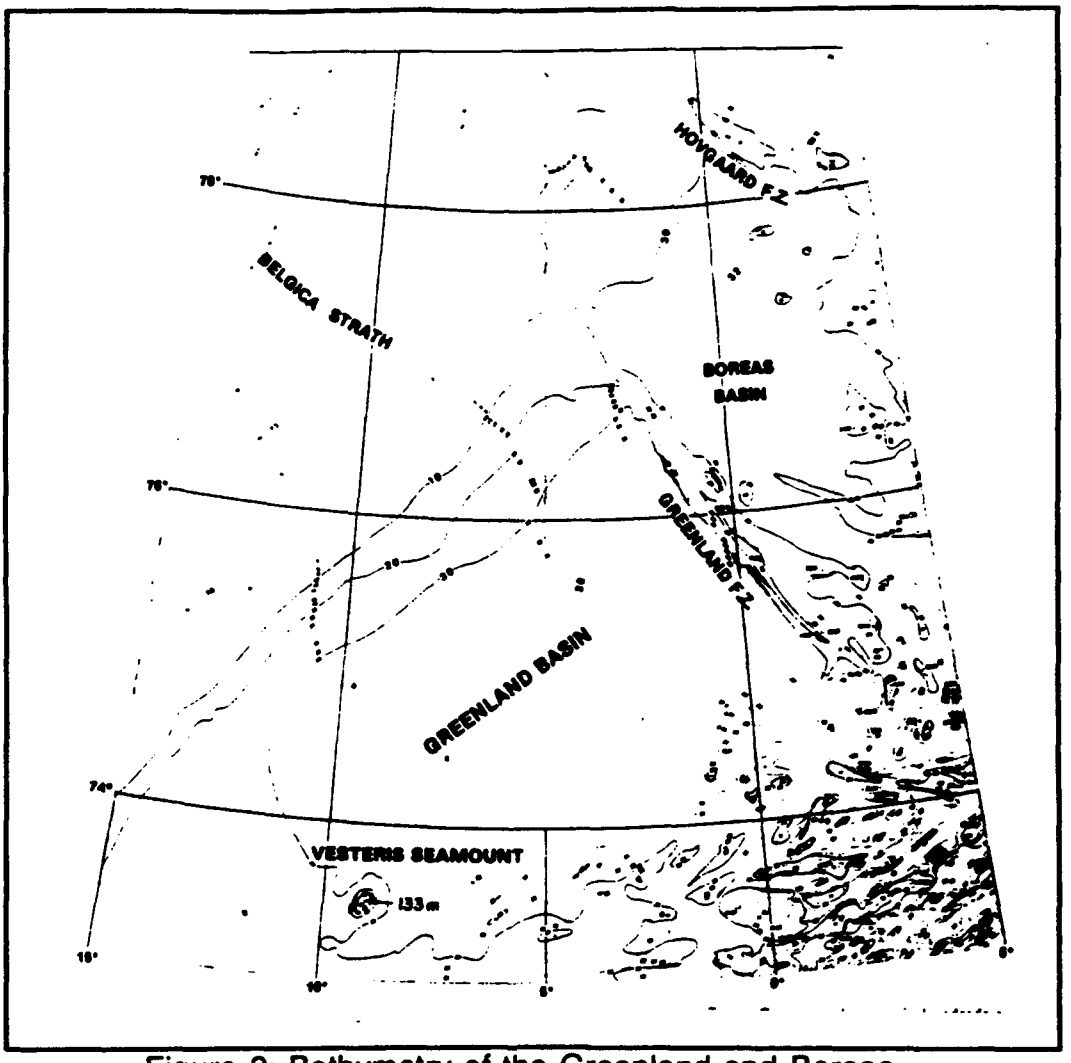

Figure 3: Bathymetry of the Greenland and Boreas Basins. Contours are in hundreds of meters (from Perry, et al., 1980)

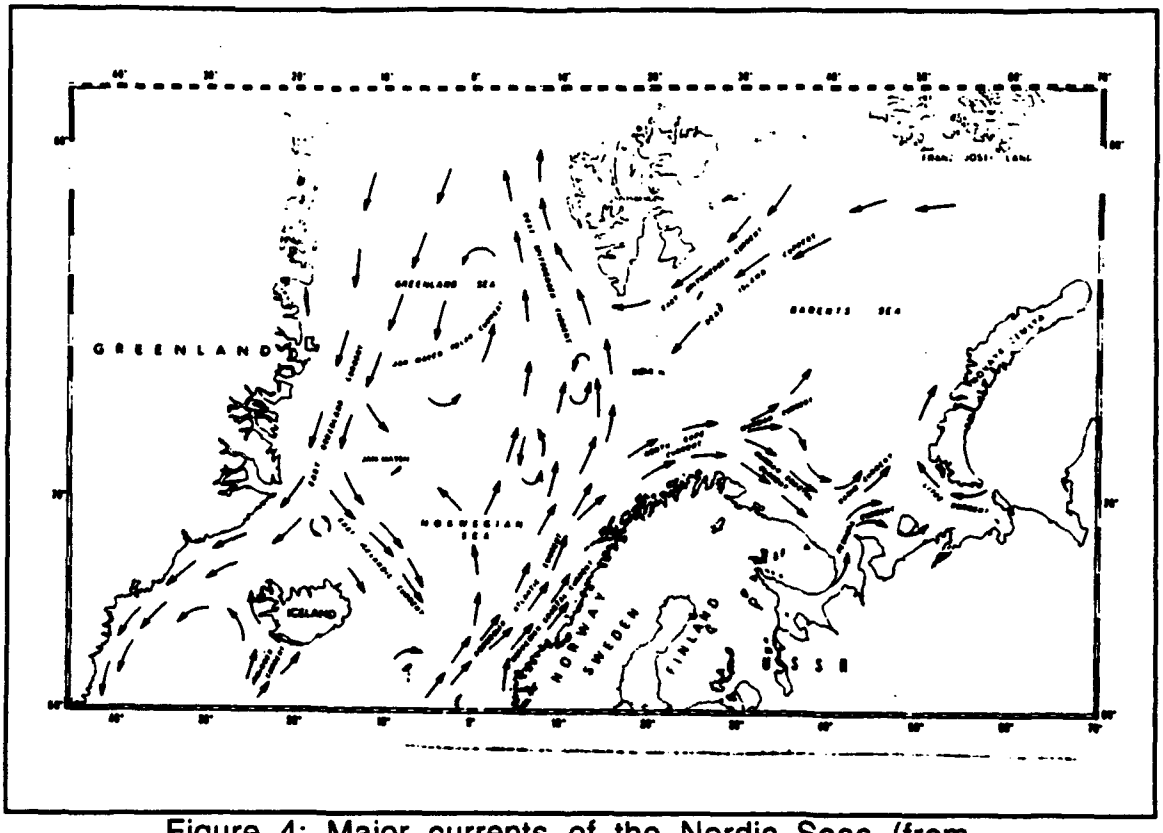

Figure 4: Major currents of the Nordic Seas (from Trengeled, 1974)

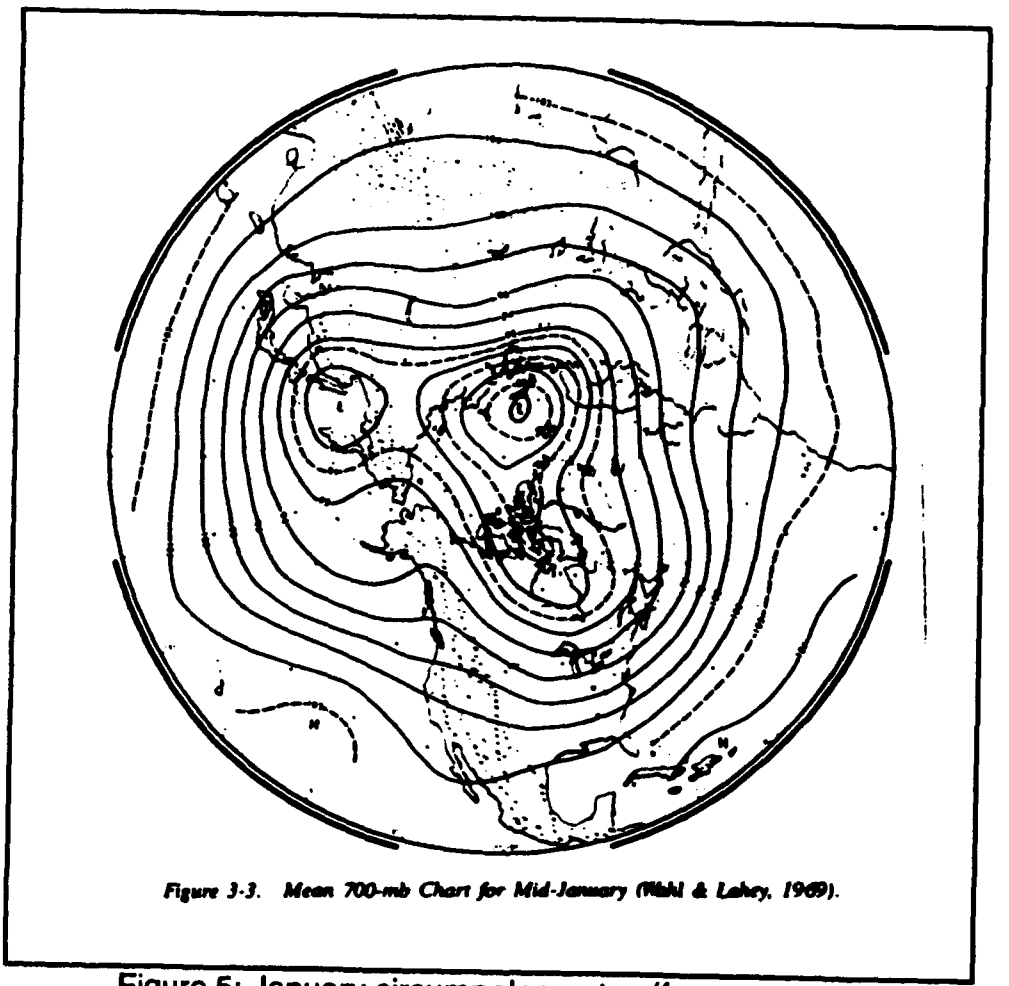

Figure 3-3. Mean 700-mb Chart for Mid-January (Wahl & Lahey, 1969).

Figure 5: January circumpolar vortex (from Sechrist et al., 1989)

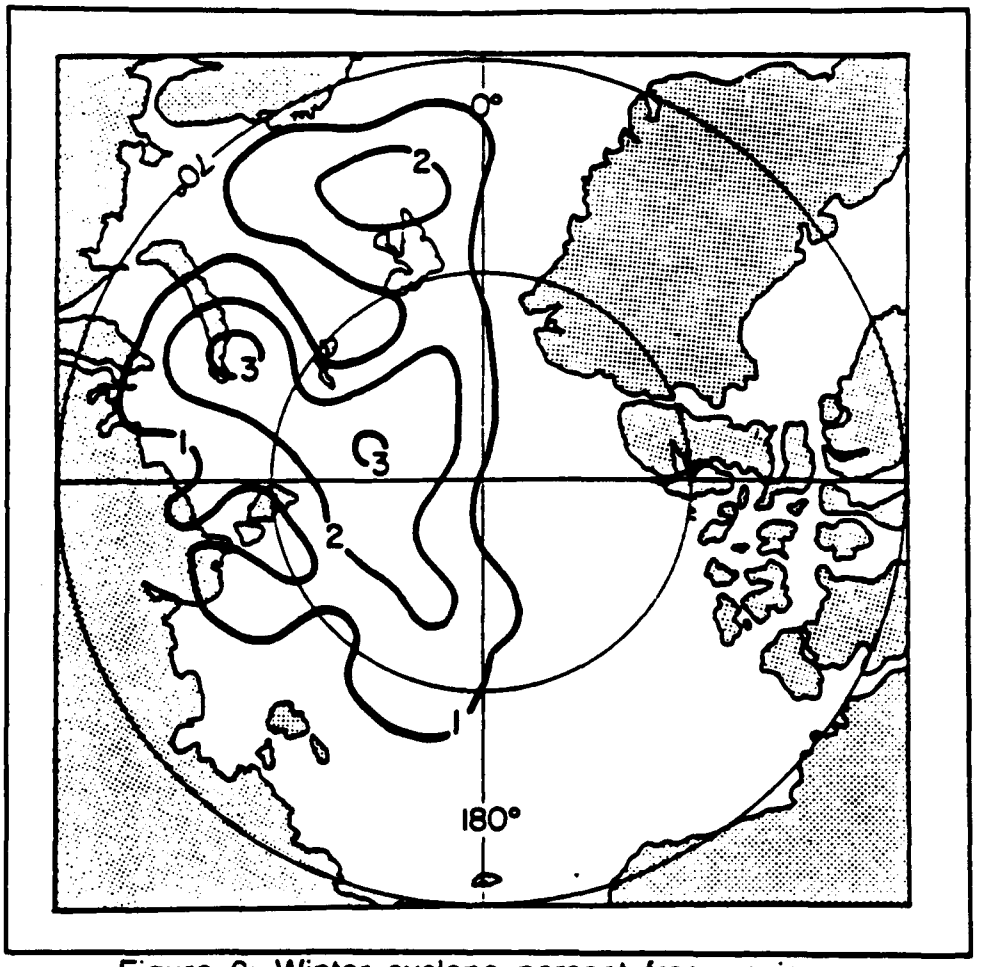

Figure 6: Winter cyclone percent frequencies, 1979-1985 (from Serreze and Barry, 1988)

II. DATA ANALYSIS

A. SIZEX METEOROLOGICAL DESCRIPTION

In order to relate strong wind events and wind shifts to changes in MIZ morphology, it is first necessary to describe the passage of high pressure and low pressure systems over the Greenland Sea during the SIZEX period. Neglecting any localized ice-sea breeze effects, strong surface winds and wind shifts are the result of high latitude cyclones transiting through the region.

A meteorological synopsis for SIZEX I was completed using several data sources. The most valuable data source was the research vessel HÄKON MOSBY, stationed near the ice edge in the Greenland Sea. Environmental observations including sea-level pressure, true wind direction and speed, relative humidity and temperature were recorded at ten minute intervals, providing a nearly continuous data set. The HÄKON MOSBY environmental observations are represented in time series format, shown in Figure 7.

National Meteorological Center (NMC) final analyses for the period 06-16 January 1992 provided a synoptic overview of the cyclones and anticyclones which influenced the direction and magnitude of the wind field in the Greenland Sea. Regional analyses from the Western Norway Forecasting Center in Bergen, Norway were used to produce a detailed description of meteorological events, including frontal positions, low pressure center positions and storm intensities. Spectral Global Model (SGM) grid point height and wind fields were used to gather observations which were not available on NMC or Norwegian final analysis charts. Meteorological analyses for the period 06-16 January 1992 are shown in Figures 8 through 28. HÄKON MOSBY's position is represented by an asterisk during periods when navigation data was available.

SIZEX I was characterized by a series of intense cyclones which closely paralleled the January climatological storm tracks as posed by Sater, et al. (1971). In each instance the low pressure center moved northeast along the Greenland coast and intensified to the lee of its high topography. In general, the storms followed one of two tracks: either they paralleled the Greenland coast to approximately 65°N, then moved eastward over Iceland and the Norwegian cape; or they continued in a northeast direction toward Spitzbergen. High pressure in the central Atlantic and the extremely cold air mass collecting on Greenland's ice shelf, with its associated high pressure/height, proved to be important factors in the meteorological conditions during the period of SIZEX I.

The SIZEX I period betweem 06-16 January can be divided into six separate events, denoted 1 through 6, based upon the HÄKON MOSBY time series and the prevailing synoptic conditions influencing the wind and pressure fields in the vicinity of HÄKON MOSBY. Period 1, 06/12Z-08/06Z, was characterized by a gradual wind shift from northeasterly early in the period to easterly by the end of the period. The ice edge during this period is visible in a ERS-1 SAR image A later section describes the ice edge in detail.

The easterly wind shift represented the passage of a 987 mb cyclone to the southeast of the ship, over the Nordic coast. The progression of the cyclone is shown in Figures 8 through 11. This low pressure system originated over the Labrador Sea and reached the east coast of Greenland near 63°N by 05/00Z. There it intensified and moved toward the East Greenland Sea. The cyclone propagated to the northeast at approximately 5 m/s. By 06/00Z it had deepened to 983 mb and reached the southeast portion of Iceland. The track of the cyclone shifted to westerly, following the upper level flow which was well-established by this period. Subsequently, the cyclone's speed of advance accelerated to 10 m/s. The low pressure center gradually filled as it crossed the Norwegian Sea

and merged with a 987 mb cyclone which had formed off the Norwegian coast by 06/21Z.. The low pressure center reached the Norwegian coast by 08/12Z with a 987 mb central pressure. HÄKON MOSBY observed north to northeasterly winds from 07/00Z-08/06Z as the cyclone passed south of her position. A decrease in surface pressure and sharp increase in wind speed at approximately 07/12Z represented the cyclone's closest point of approach to the ship.

Period 2, 08/06Z-09/06Z, represented a time of transition between low pressure systems that propagated across the Greenland and Norwegian Seas. The ice edge during this period is clearly delineated in a ERS-1 SAR image obtained during an ascending orbit.

The period was characterized by high pressure relative to the preceding time frame, and weak-to-moderate westerly and northwesterly winds over HÄKON MOSBY. Figures 12 and 13 illustrate the movement of high pressure into the region. As the 987 mb cyclone reached the Norwegian coast and moved over northern Europe, high pressure over the mid-Atlantic Ocean began ridging northward toward the Greenland Sea. By 08/12Z the ridge was well-established to the south of Iceland. High pressure over the Greenland Sea proved to be a short-lived event, as a strong cyclone was developing over the Labrador Sea, upstream of the ridge. A decrease in sea-level pressure and a abrupt shift to southwesterly flow marked the end of this period as the next low pressure system approached.

Period 3, 09/06Z-12/00Z, represented a period of strong ice edge forcing by the wind field as a deep low pressure system tracked across the Greenland Sea. Two SAR images of the ice edge (one descending and one ascending) were available over this period.

As the cyclone tracked eastward and passed to the south, winds over HÄKON MOSBY shifted from southwesterly to northeasterly. Figures 14 through

19 describe the translation and development of this low pressure system. The cyclone originated over the Labrador Sea and advanced northeast at speeds of 12-13 m/s. It continued to deepen and move to the northeast over the period 09/00Z-10/00Z , attaining a central pressure of 976 mb. Hence, this low pressure system in conjunction with high pressure ridging to the east, resulted in an abrupt wind shift to southwesterly flow at HÄKON MOSBY'S position by 09/06Z. By 09/12Z a low pressure trough extended to the northeast and a secondary 990 mb low pressure had formed near 72°N/15°W. The cyclones propagated towards the northeast and effectively combined to form a 958 mb low pressure center over the Greenland Sea by 10/12Z. The low pressure center's trajectory changed from northeastward to eastward. In response to the movement of the low pressure system, winds shifted to easterly over the HÄKON MOSBY. High pressure over the Greenland plateau was displaced northward. Wind speeds increased at HÄKON MOSBY'S position, with a maximum wind of 20 m/s attained at 10/00Z as a large pressure gradient was established between the cyclone and high pressure over the central Arctic Ocean. They remained in excess of 13 m/s until 11/12Z, as the cyclone's speed of advance slowed and high pressure persisted over the central Arctic Ocean.

HÄKON MOSBY observed a wind shift to northeasterly at approximately 10/18Z, when the cyclone passed to the south of her position. By 11/12Z the cyclone had tracked southeast of HÄKON MOSBY and reached the Norwegian cape, where it began to weaken. Winds rapidly diminished after 11/12Z as the cyclone moved over the Kola Peninsula and high pressure ridged into the region. The residence time associated with this storm system was longer than others--approaching 48 hours, likely the result of the cyclone's reduced speed of advance between 10/00Z and 11/12Z. By 12/00Z it was sufficiently inland that it no longer influenced the surface flow in the vicinity of the HÄKON MOSBY.

Period 4, 12/00Z-13/00Z, represented the ridging of high pressure west of the British Isles northward into the Greenland Sea. Figures 20 and 21 describe synoptic situation during this period. The winds over HÄKON MOSBY abruptly shifted to southwesterly and diminished as the low pressure system moved across northern Europe and high pressure ridged over her position. Winds steadily increased from 12/00Z to 12/18Z, attaining a maximum speed of 12 m/s. It is probable that the increase in wind speed was attributed to an enhanced pressure gradient caused by the approach of another low pressure center along the eastern edge of Greenland. HÄKON MOSBY observed a gradual wind shift to southerly flow by 13/00Z as the ridge was displaced eastward over the Norwegian coast by the approaching cyclone. A corresponding decrease in sea-level pressure at HÄKON MOSBY between 12/12Z and 13/00Z was consistent with the movement of the ridge.

Period 5, from 13/00Z to 13/21Z, represented the approach of a intense low pressure system towards HÄKON MOSBY's position. There was one ERS-1 SAR image obtained in a descending orbit during this period. Figures 21-23 show the propagation and development of this system.

Observed winds over HÄKON MOSBY shifted from southerly to easterly and steadily increased in speed, reaching 18 m/s by the end of period 5. This low pressure center had entered the Greenland Sea by 13/00Z and had weakened substantially to 1000 mb. The cyclone proceeded to the northeast at 6 m/s following the low-level and mid-level steering flow. As the cyclone progressed over the Greenland Sea it deepened; possibly in response to warm air advection from the south. Surface pressures at HÄKON MOSBY's position began falling rapidly as the low pressure system approached. Winds were southeasterly at 8 m/s in advance of the system and then shifted to easterly as the system neared its closest point of approach. Winds continually increased in response to the

enhanced pressure gradient between the advancing/developing cyclone and building high pressure over Greenland and the Arctic basin. By 13/12Z the system had divided into two separate 990 mb low pressure centers and accelerated to 15 m/s, becoming the dominant feature over the Greenland Sea. They followed the 850 mb and 700 mb flow, continuing to the northeast. By 13/21Z the northernmost cyclone was over HÄKON MOSBY's position and had further intensified to 976 mb. Winds increased to 16 m/s and shifted to easterly as the cyclone passed slightly south of her position.

Winds shifted from easterly to northwesterly over period 6, from 13/21Z to 14/21Z, as the low pressure system intensified and tracked to the east. A 14/20Z ERS-1 SAR image of the ice edge was obtained in an ascending orbit. High pressure present over the central Arctic Ocean and Greenland created a strong pressure gradient over the northern Greenland Sea. HÄKON MOSBY recorded northerly winds in excesss of 25 m/s by 14/12Z as the cyclone passed her position. Figures 23-28 depict the passage of this system. The residence time associated with this storm system was estimated to be 24 hours as the cyclone tracked across Spitzbergen and entered the Barents Sea. Northwesterly flow persisted over HÄKON MOSBY through 16/12Z as the speed of advance of this low pressure system slowed to approximately 5 m/s. Wind speeds over the ice edge decreased gradually after 14/12Z as the cyclone proceeded to the east and high pressure began ridging into the region.

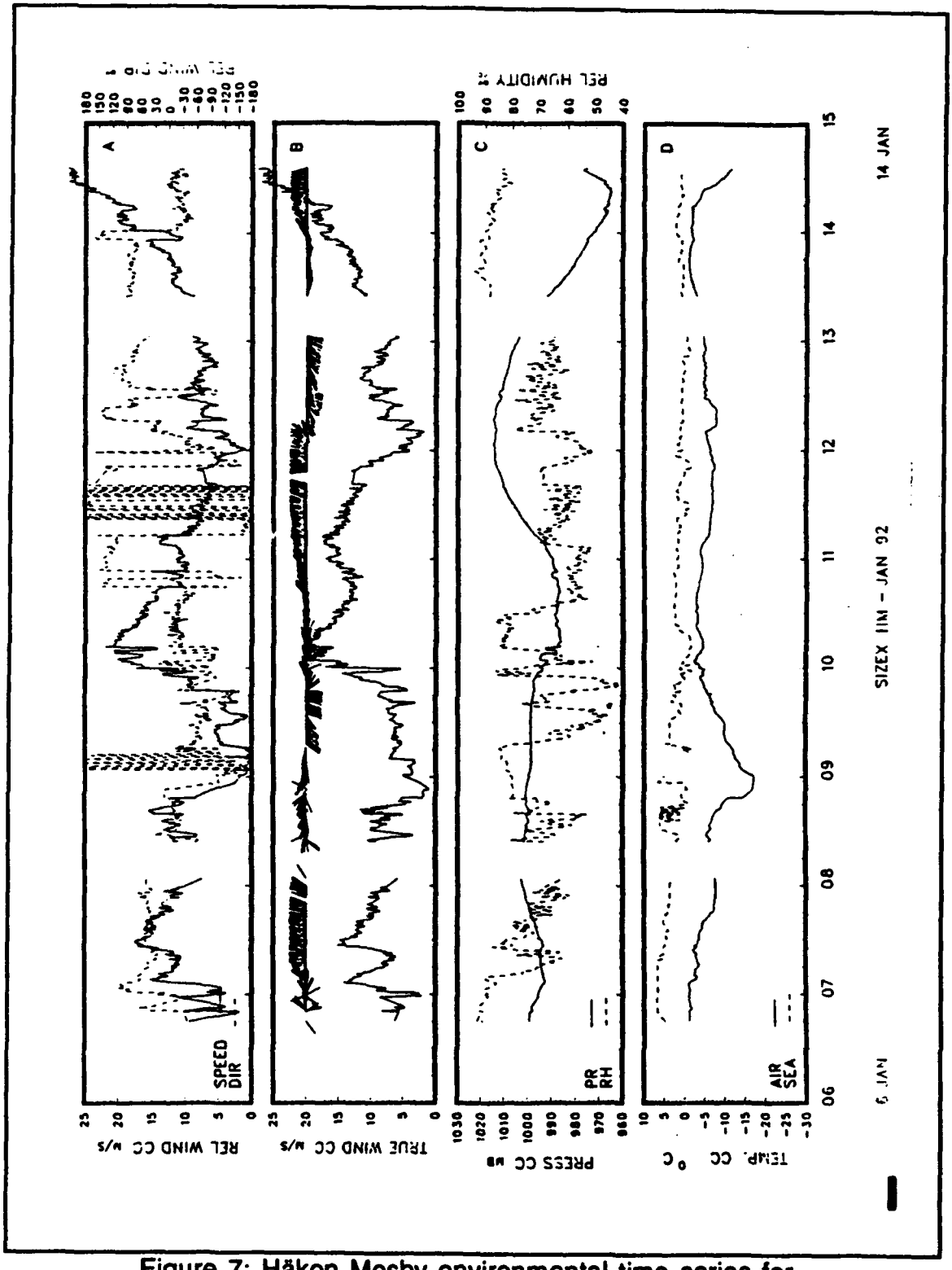

Figure 7: Häkon Mosby environmental time series for the period 07-15 January 1992, based on observations taken at 10 minute intervals.

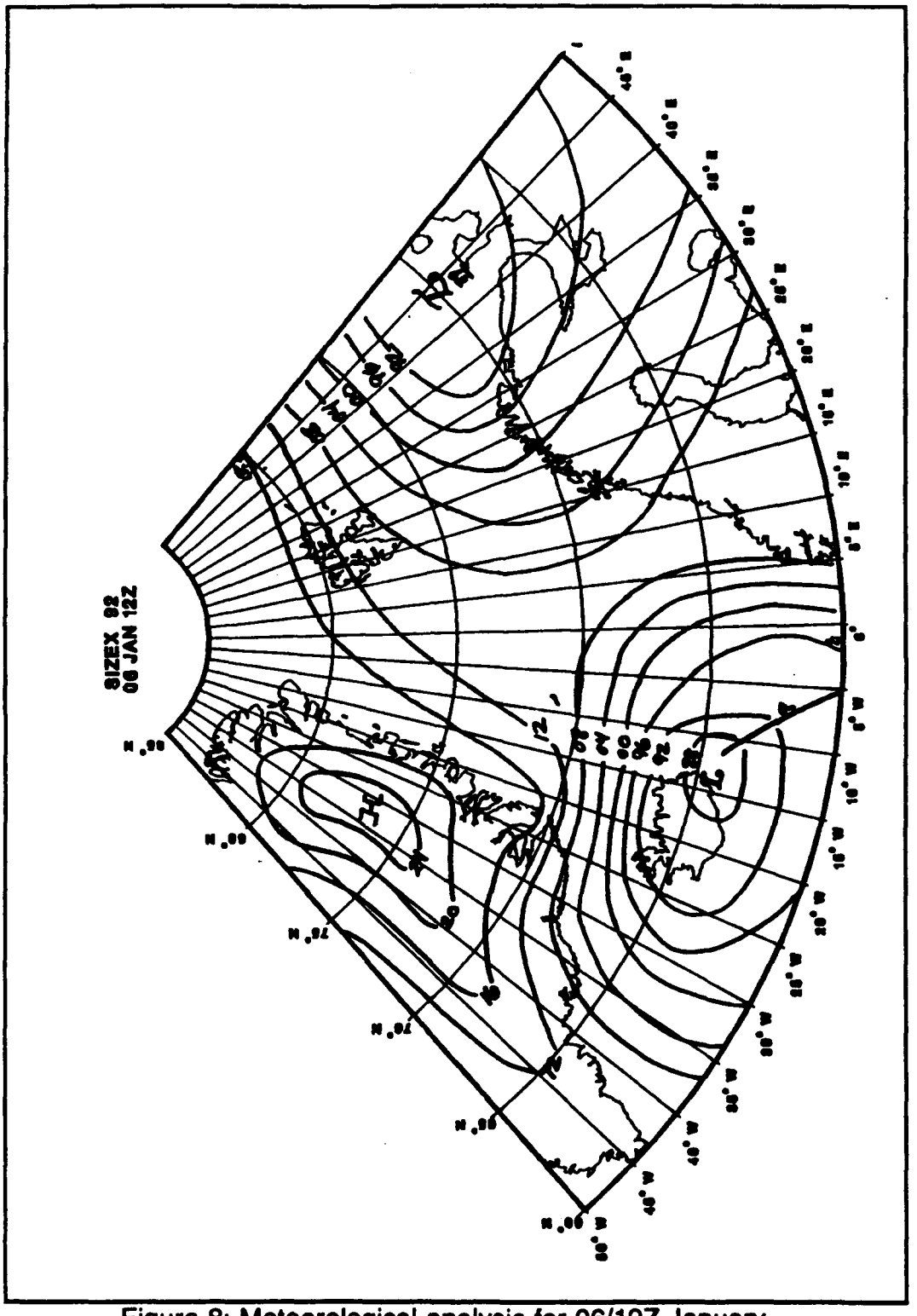

Figure 8: Meteorological analysis for 06/12Z January 1992.

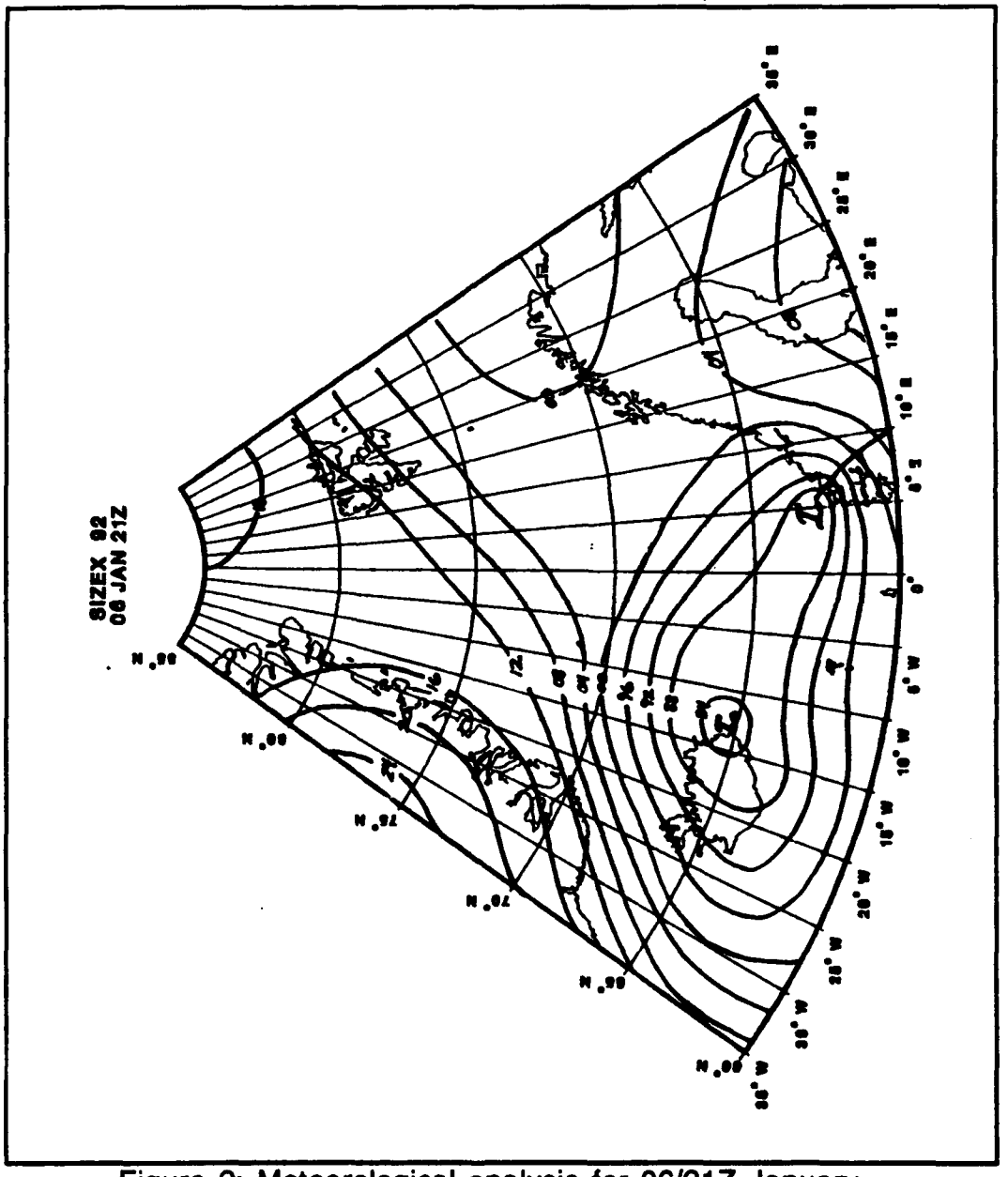

Figure 9: Meteorological analysis for 06/21Z January 1992

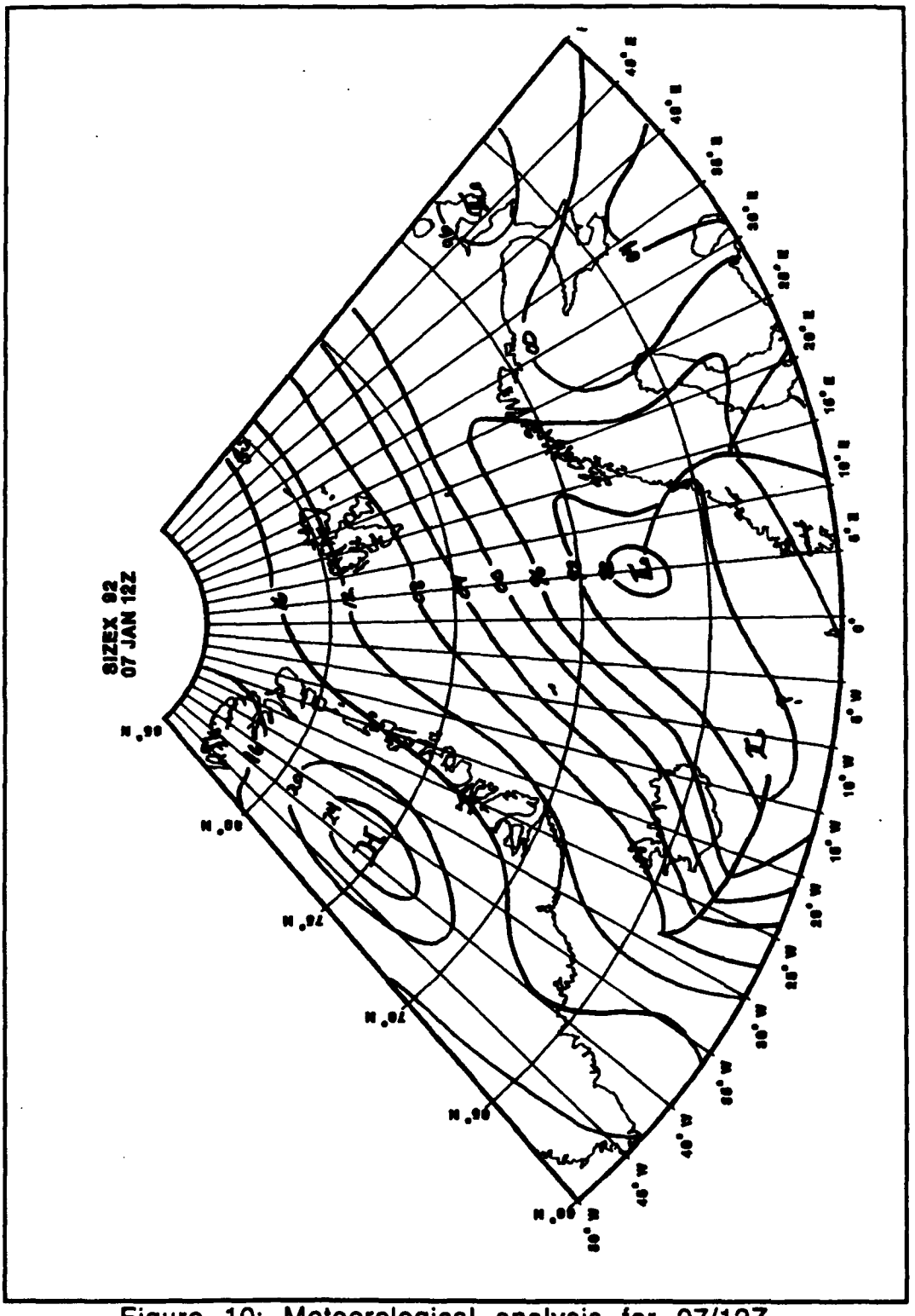

Figure 10: Meteorological analysis for 07/12Z January 1992

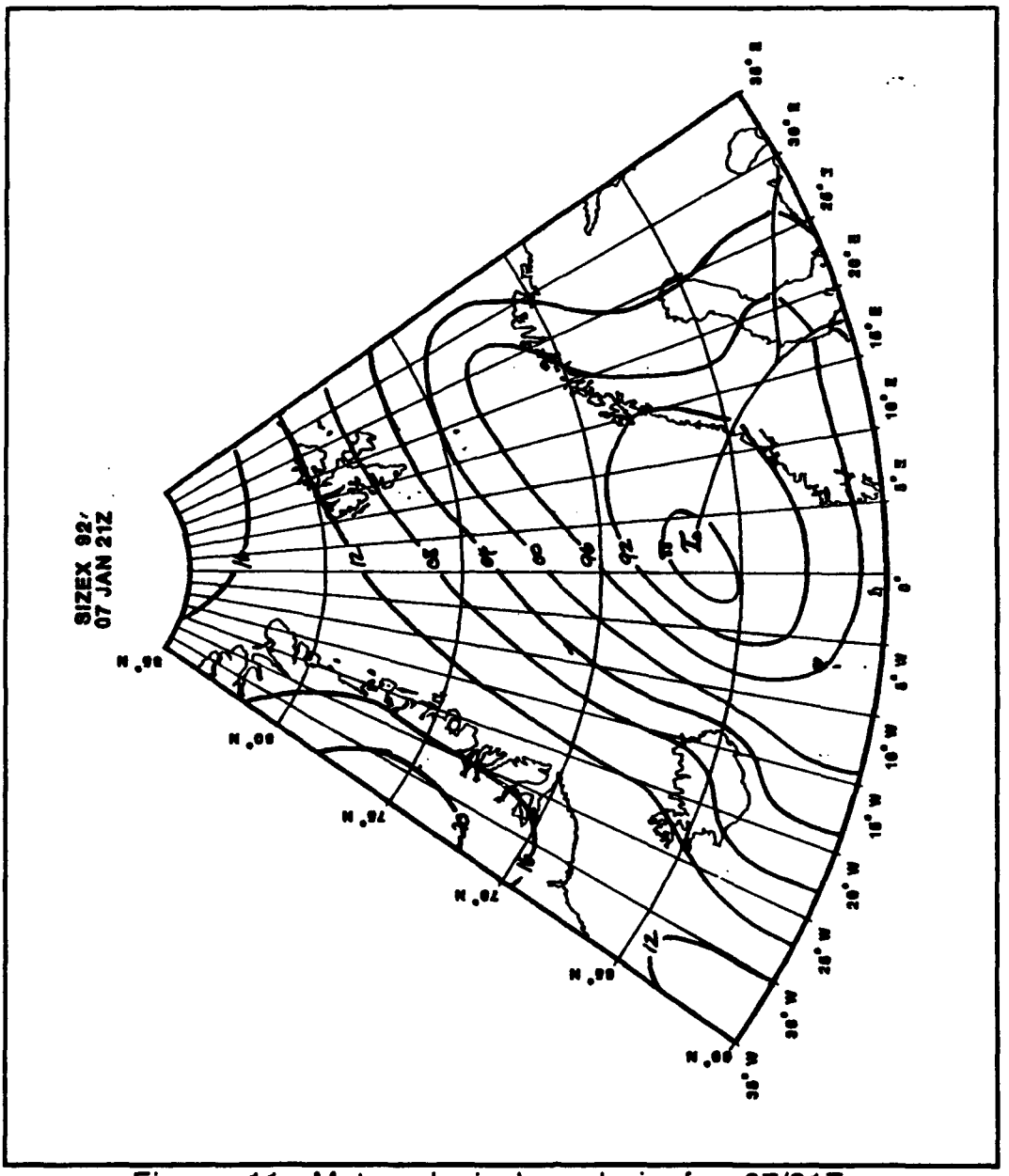

Figure 11: Meteorological analysis for 07/21Z January 1992

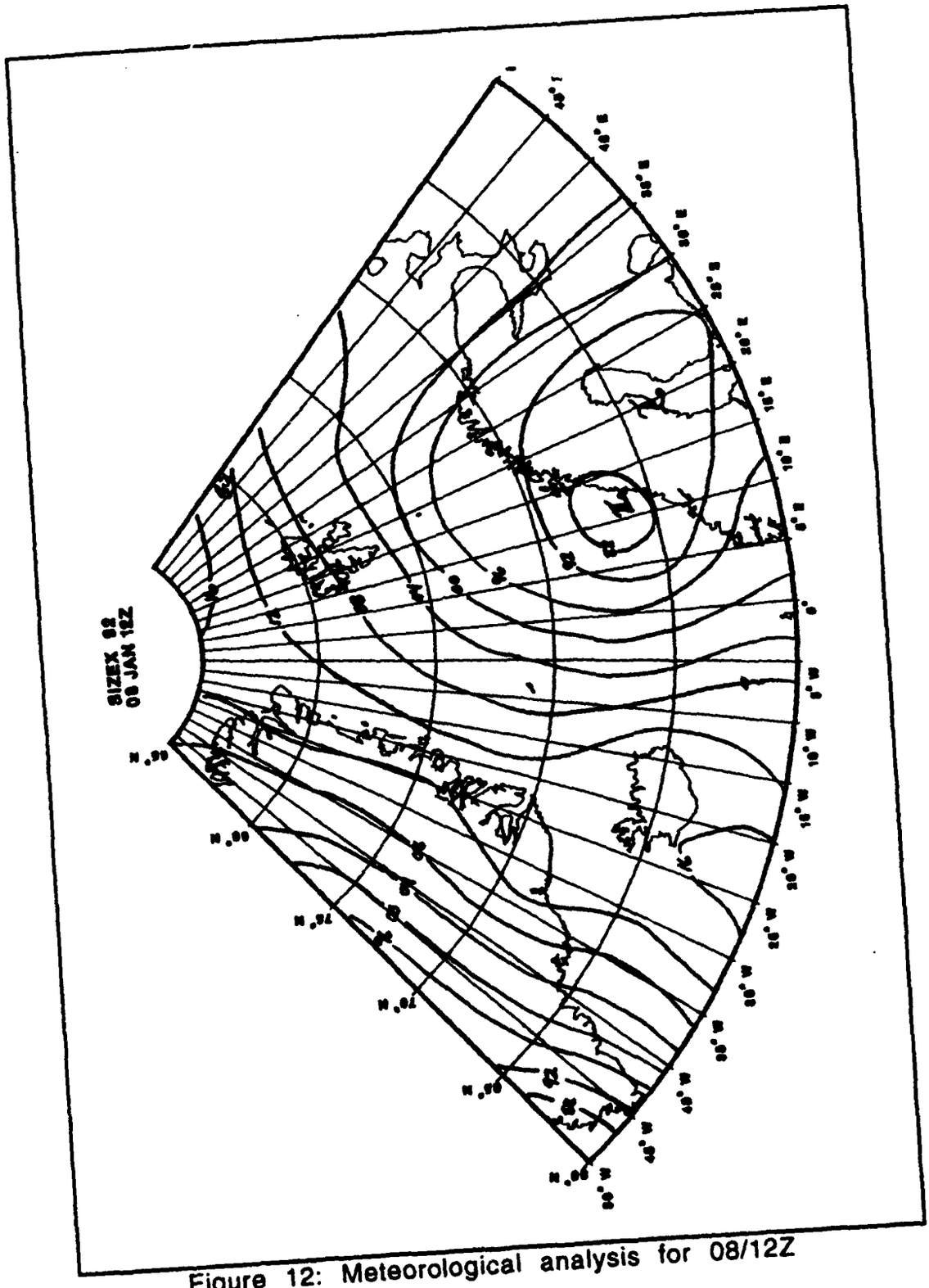

Figure 12: Meteorological analysis for 08/12Z January 1992

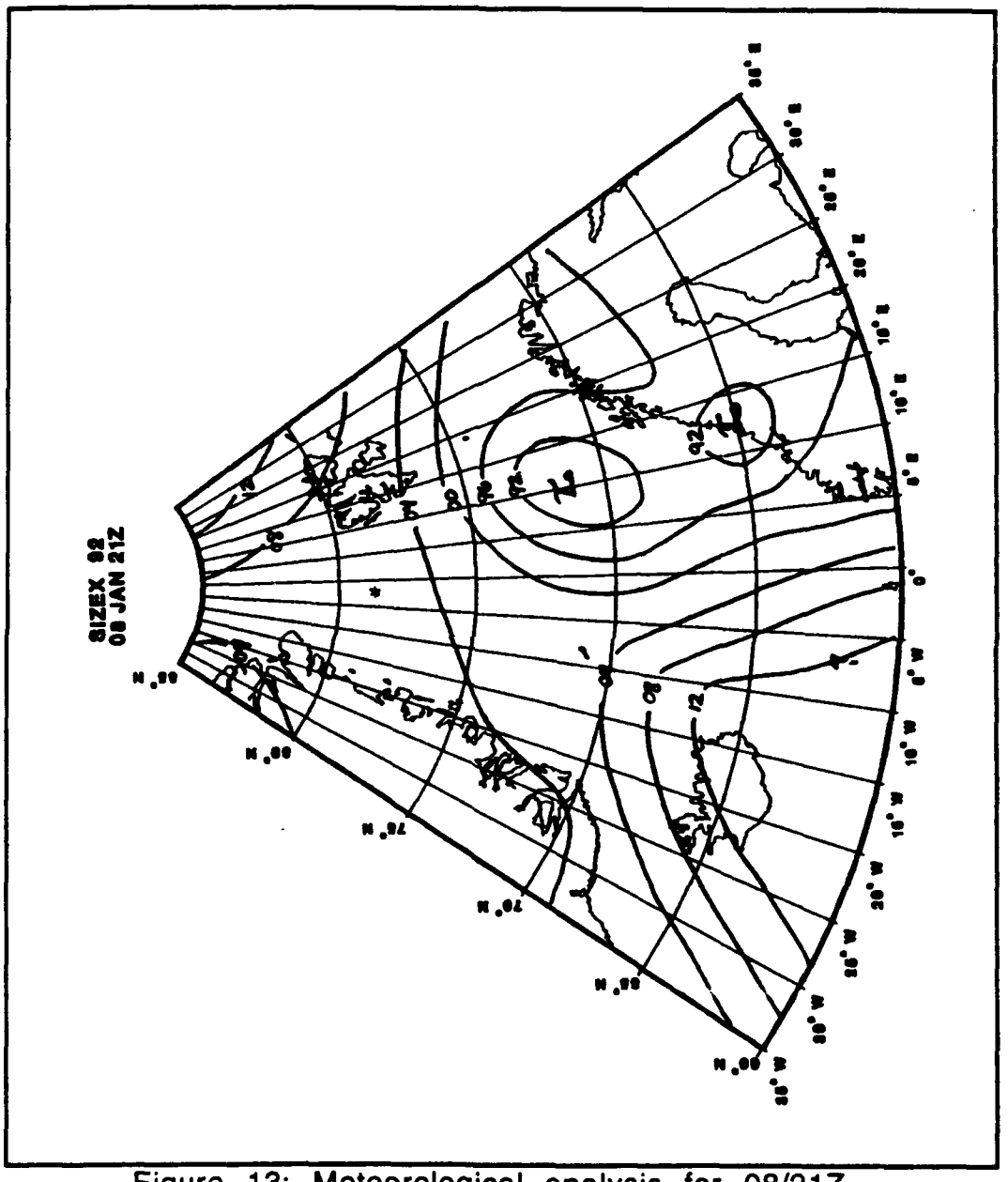

Figure 13: Meteorological analysis for 08/21Z January 1992. Häkon Mosby's position is denoted by a "*" on the chart.

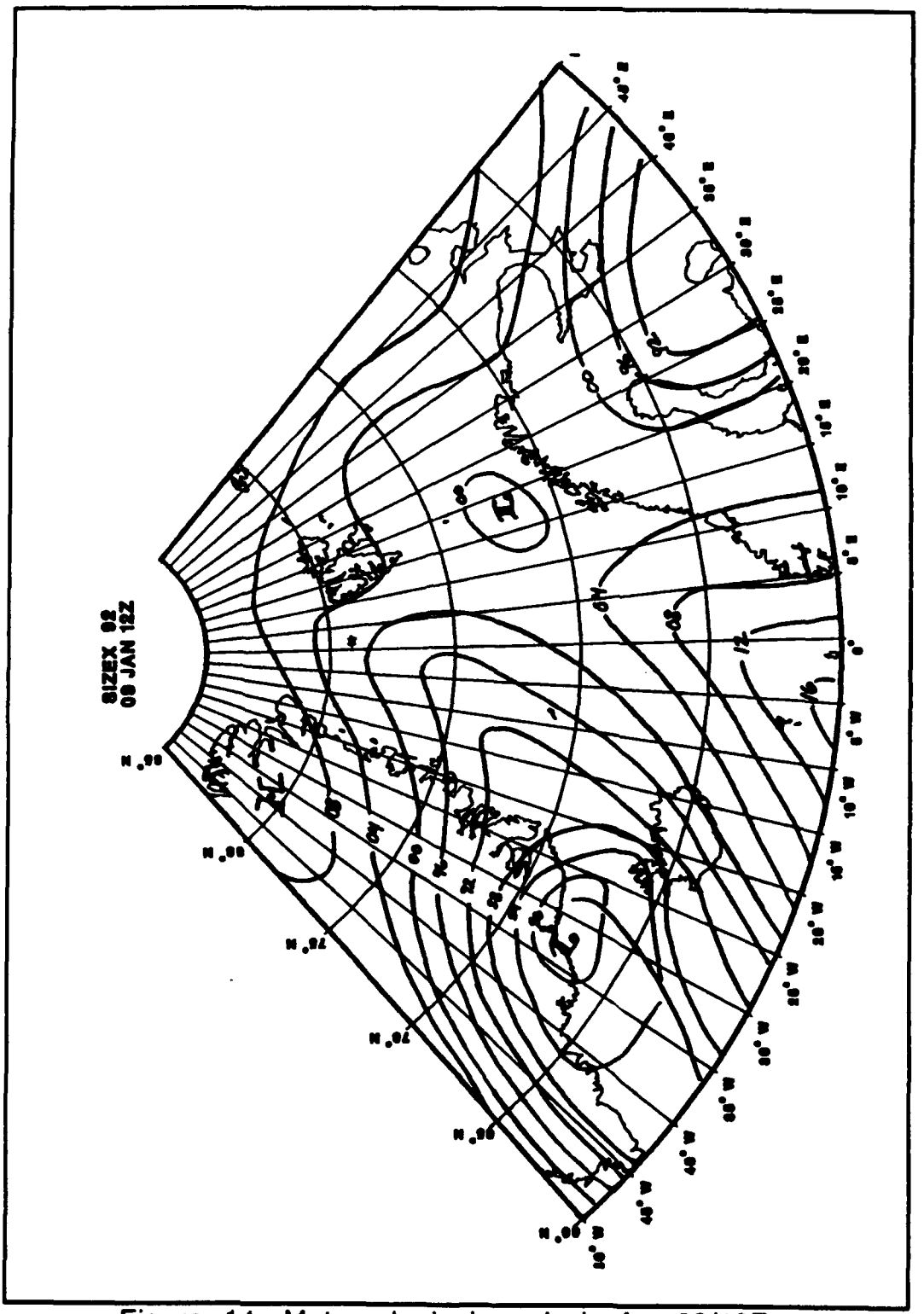

Figure 14: Meteorological analysis for 09/12Z January 1992. Häkon Mosby's position is denoted by a "*" on the chart.

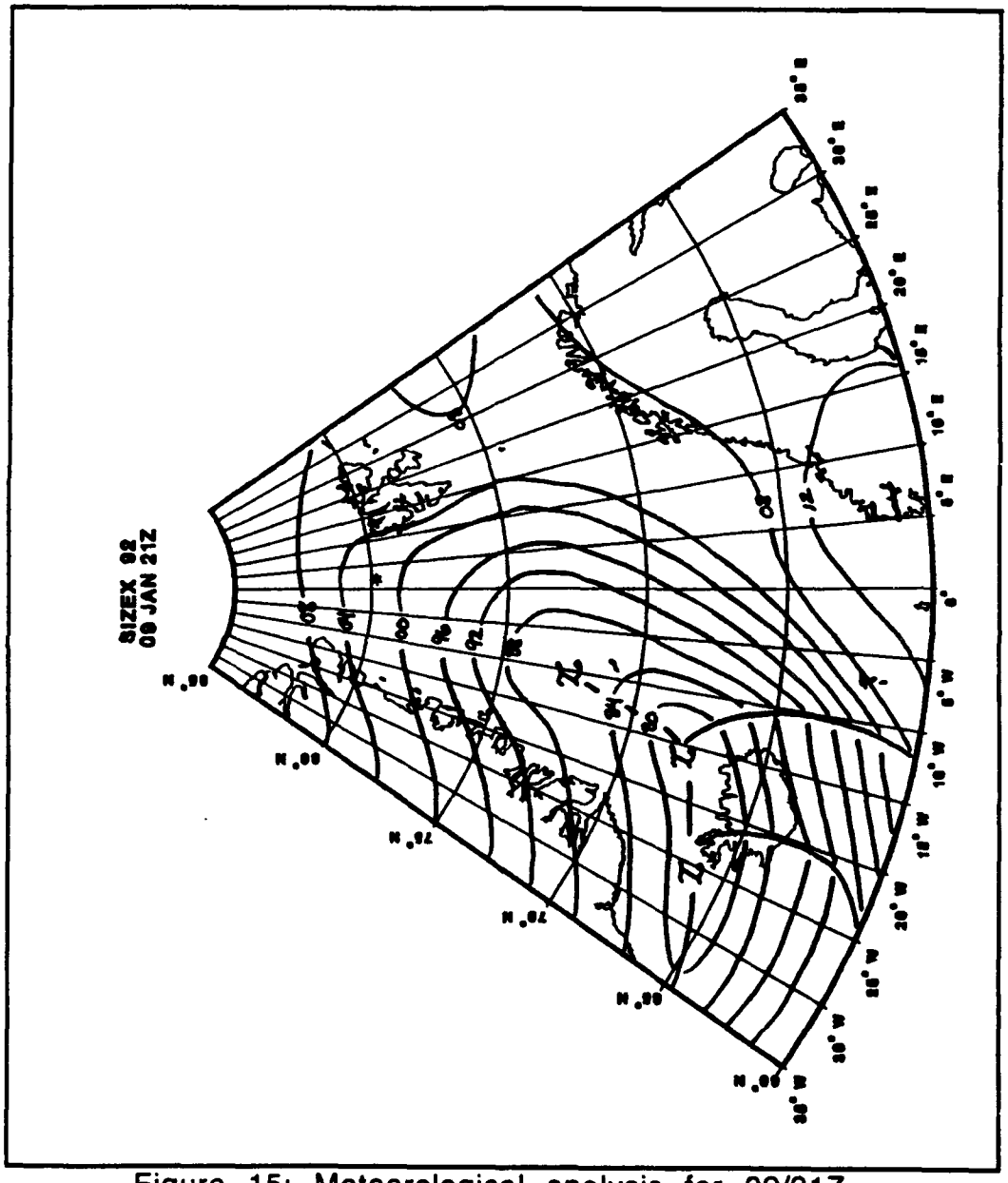

Figure 15: Meteorological analysis for 09/21Z January 1992. Häkon Mosby's position is denoted by a "*" on the chart.

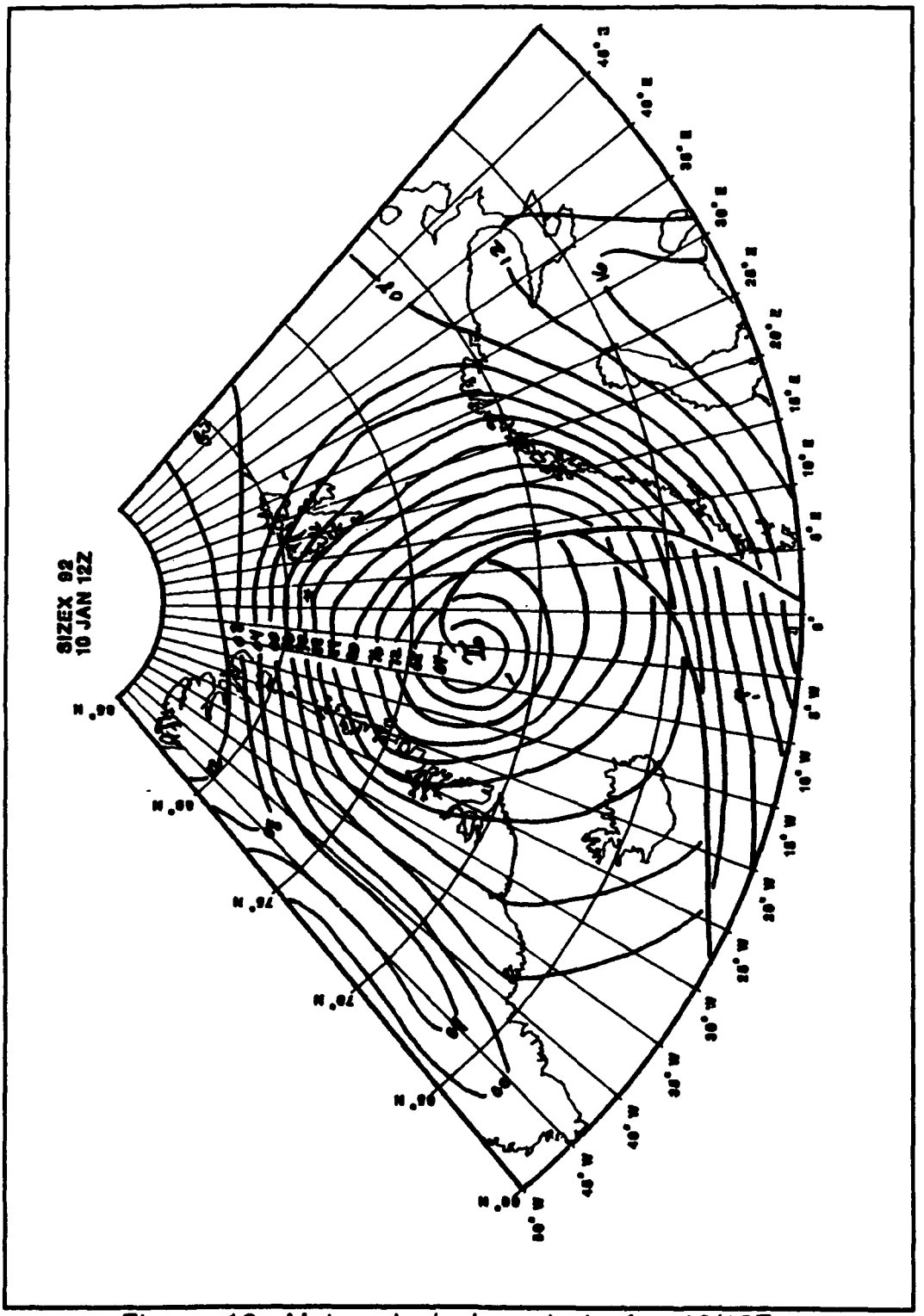

Figure 16: Meteorological analysis for 10/12Z January 1992. Häkon Mosby's position is denoted by a "*" on the chart.

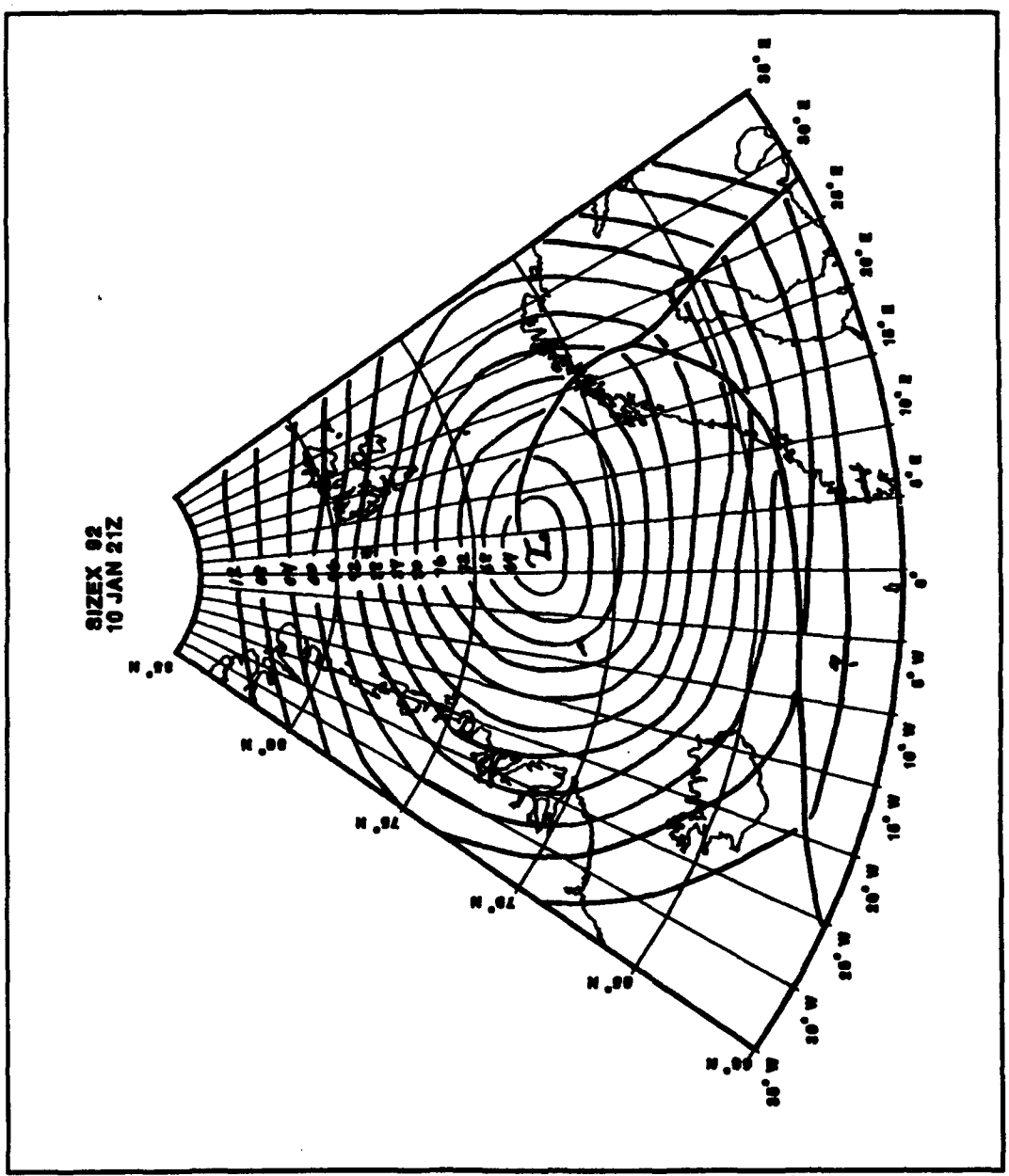

Figure 17: Meteorological analysis for 10/21Z January 1992. Häkon Mosby's position is denoted by a "*" on the chart.

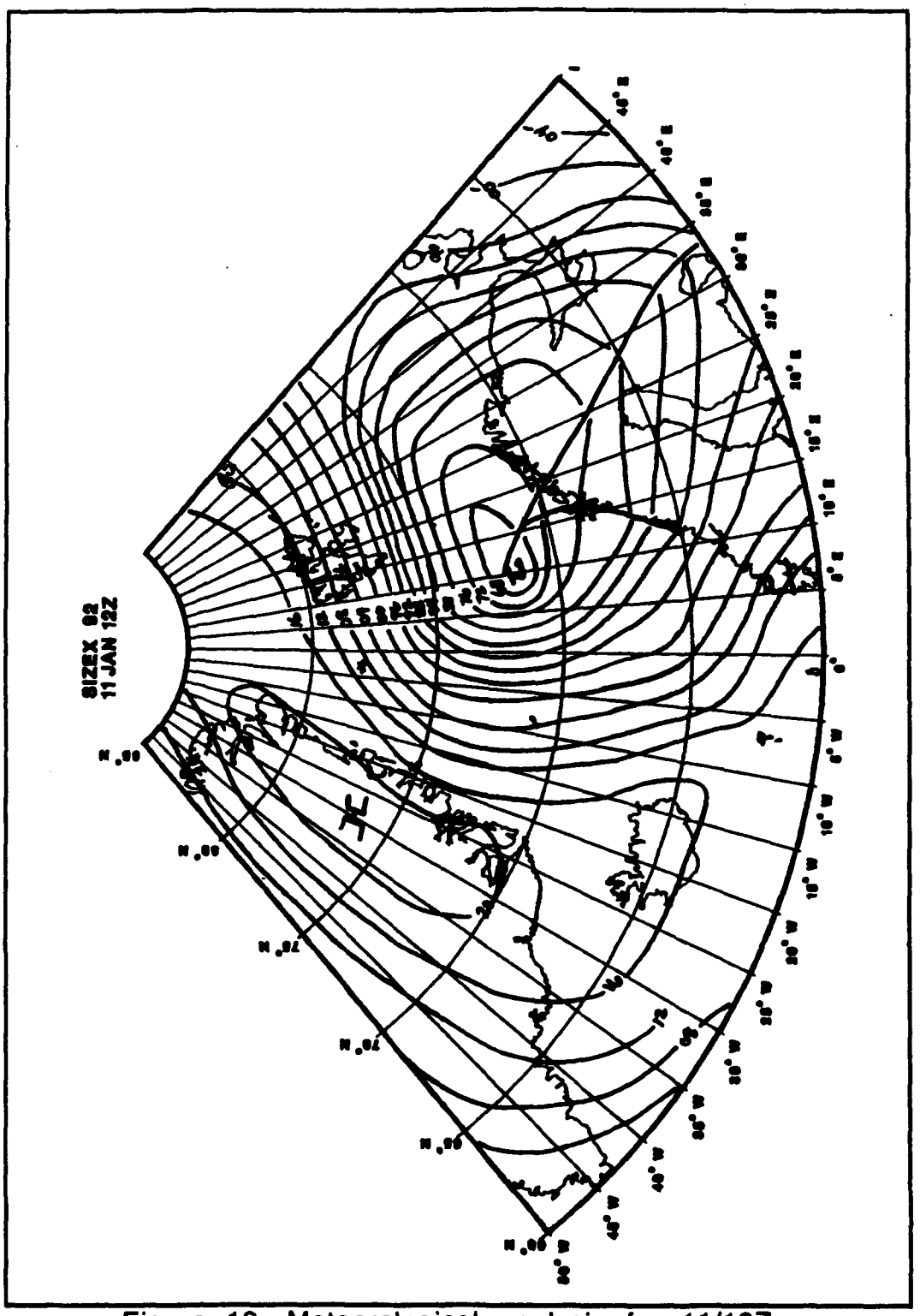

Figure 18: Meteorological analysis for 11/12Z January 1992. Häkon Mosby's position is denoted by a "*" on the chart.

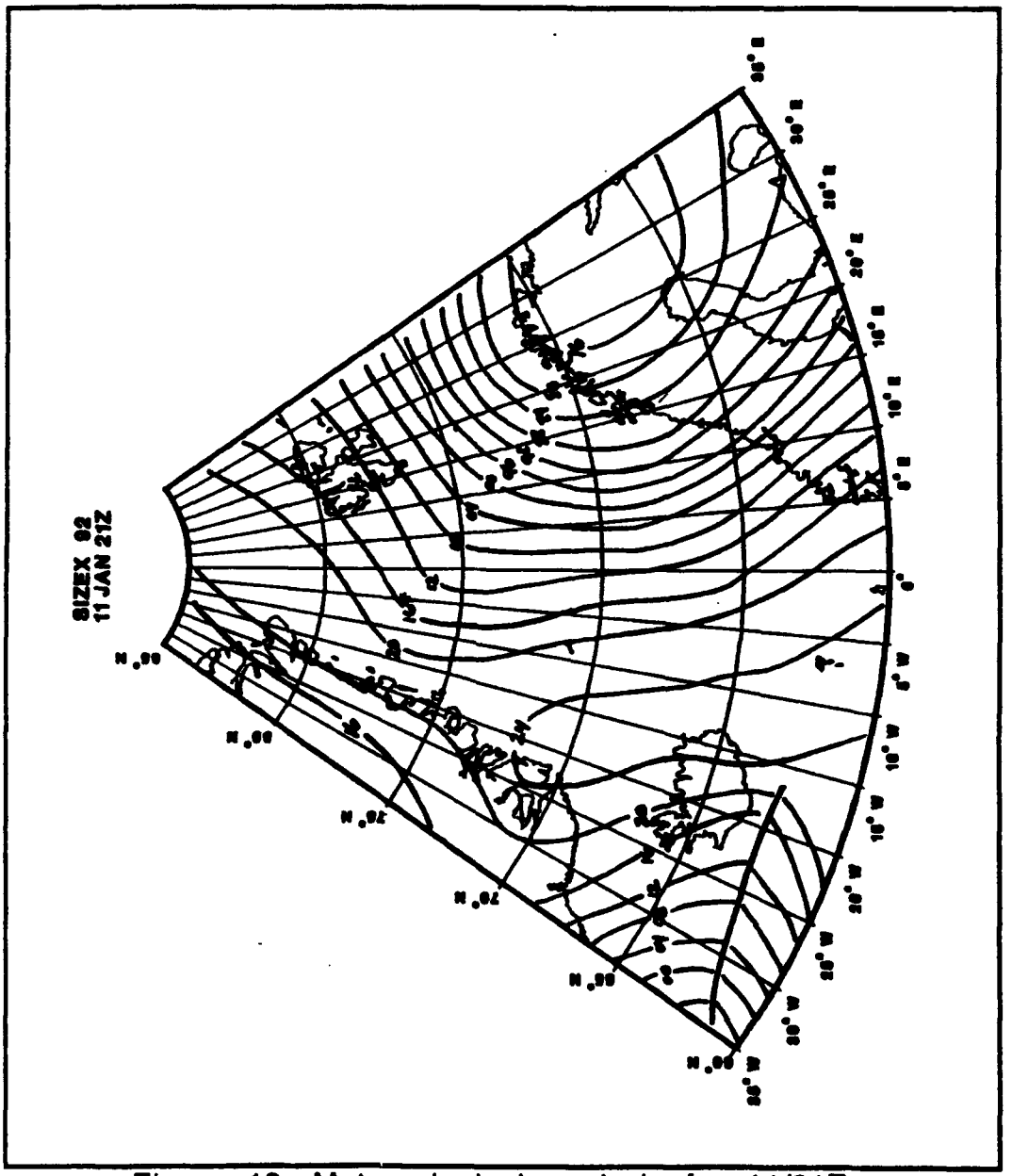

Figure 19: Meteorological analysis for 11/21Z January 1992. Håkon Mosby's position is denoted by a "*" on the chart.

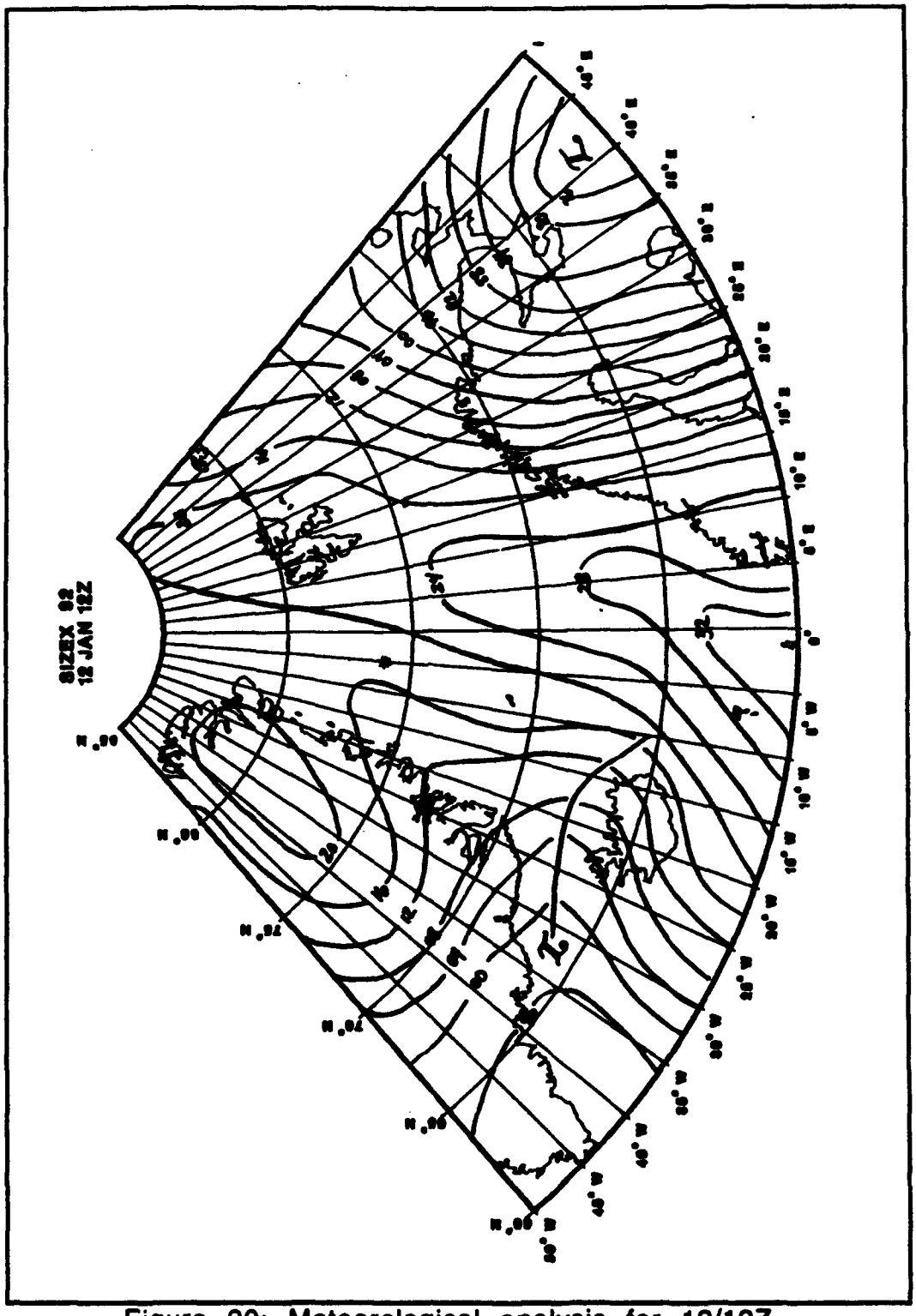

Figure 20: Meteorological analysis for 12/12Z January 1992. Häkon Mosby's position is denoted by a "*" on the chart.

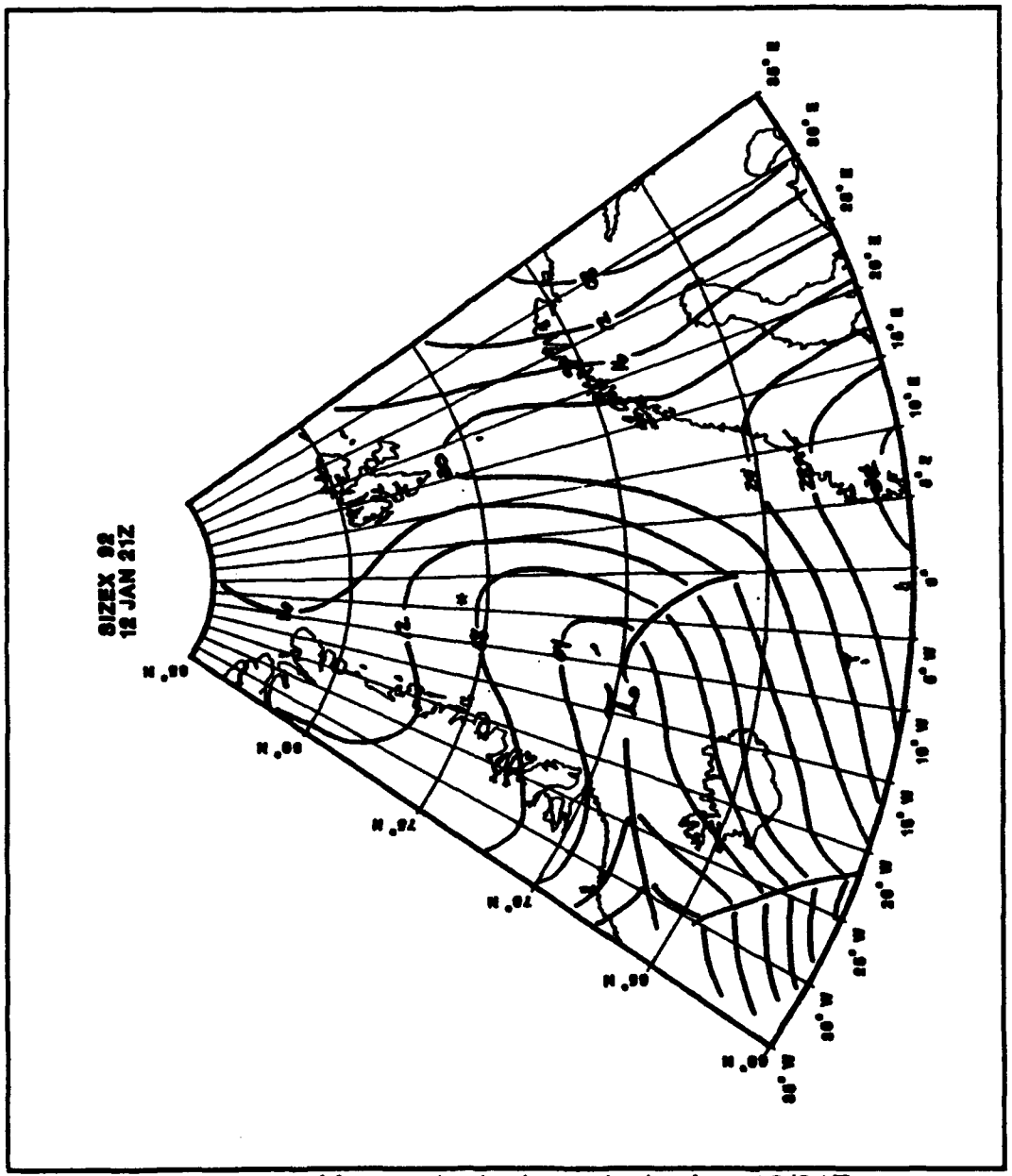

Figure 21: Meteorological analysis for 12/21Z January 1992. Häkon Mosby's position is denoted by a "*" on the chart.

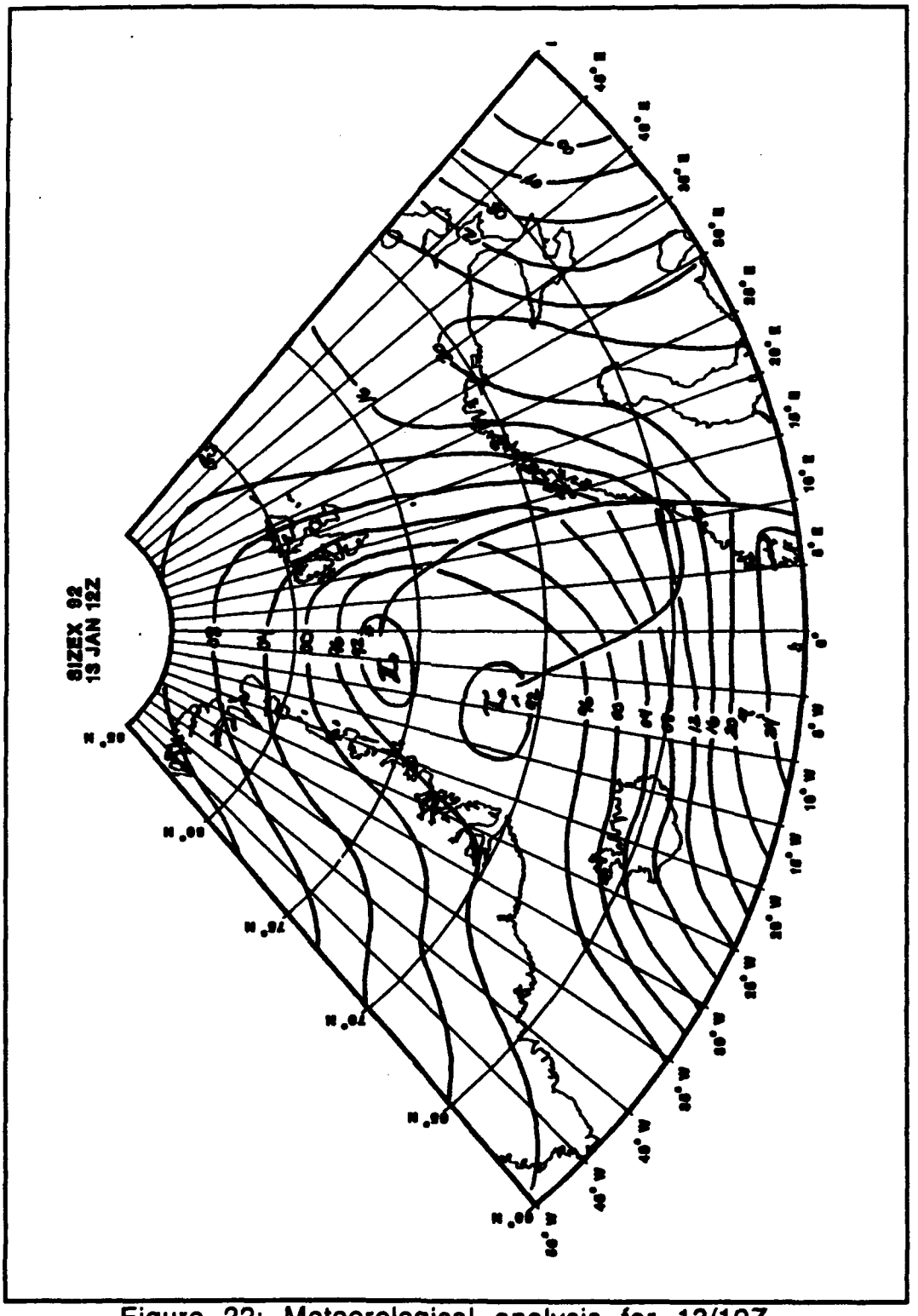

Figure 22: Meteorological analysis for 13/12Z January 1992. Häkon Mosby's position is denoted by a "*" on the chart.

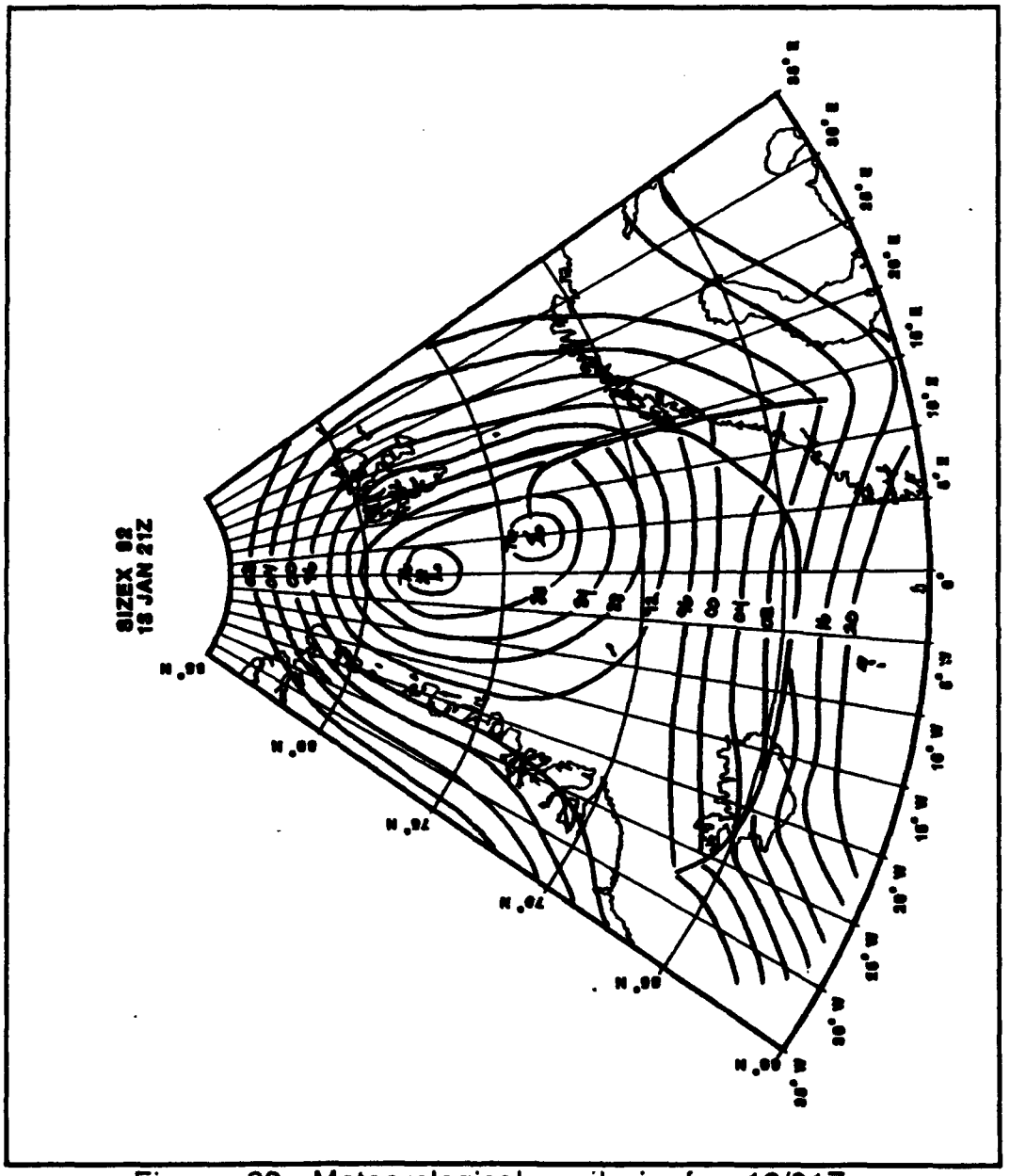

Figure 23: Meteorological analysis for 13/21Z January 1992. Häkon Mosby's position is denoted by a "*" on the chart.

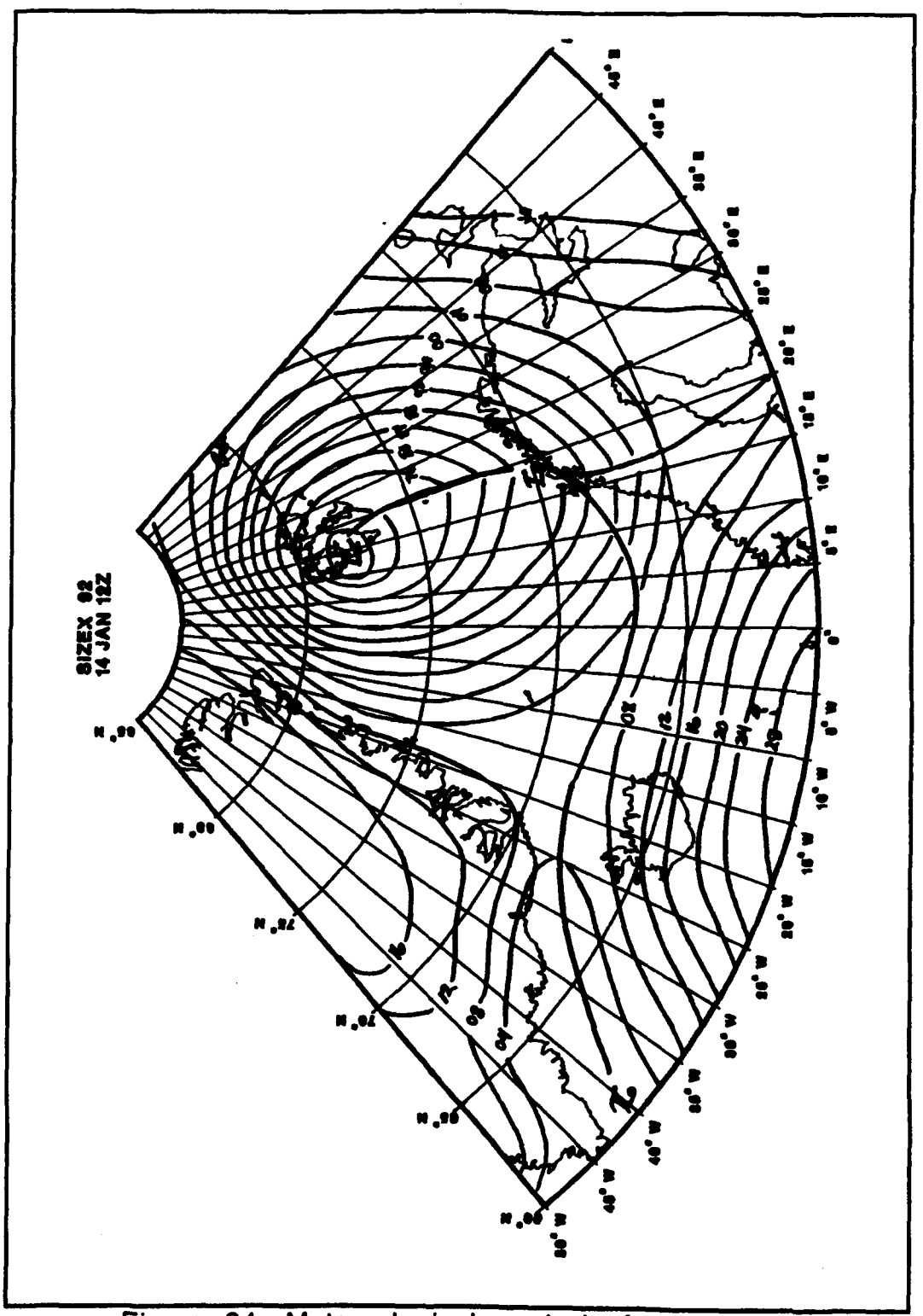

Figure 24: Meteorological analysis for 14/12Z January 1992. Häkon Mosby's position is denoted by a "*" on the chart.

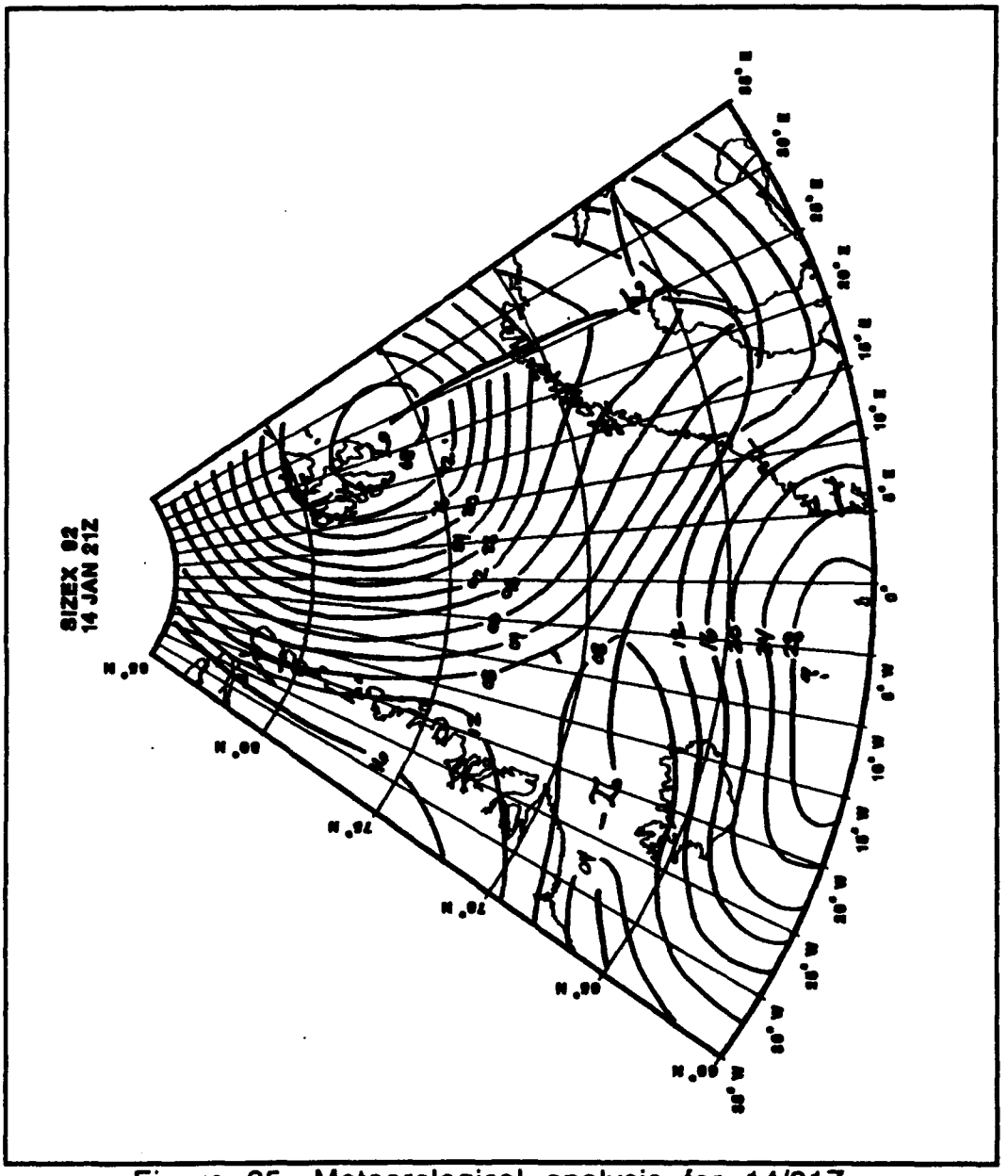

Figure 25: Meteorological analysis for 14/21Z January 1992. Häkon Mosby's position is denoted by a "*" on the chart.

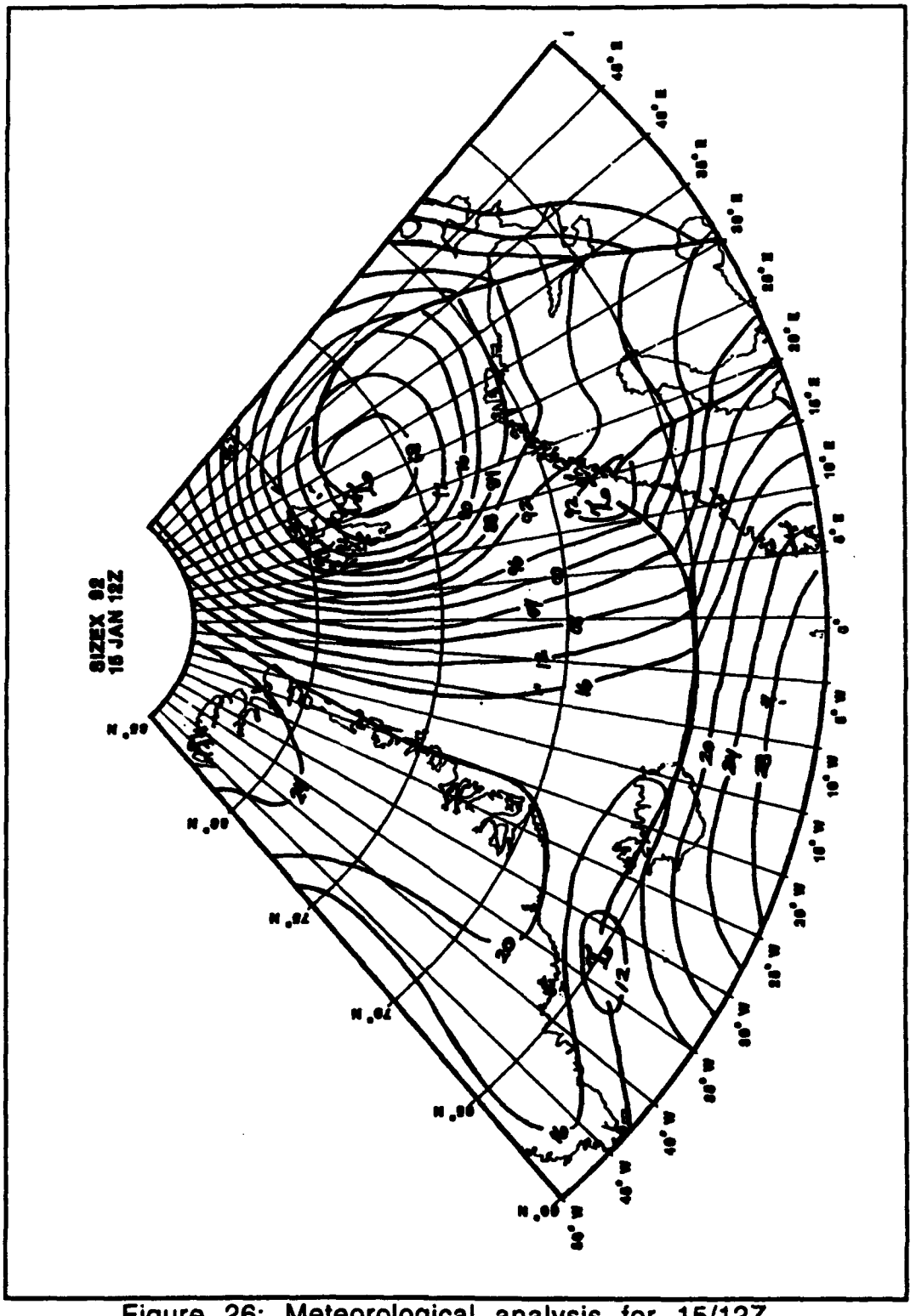

Figure 26: Meteorological analysis for 15/12Z January 1992.

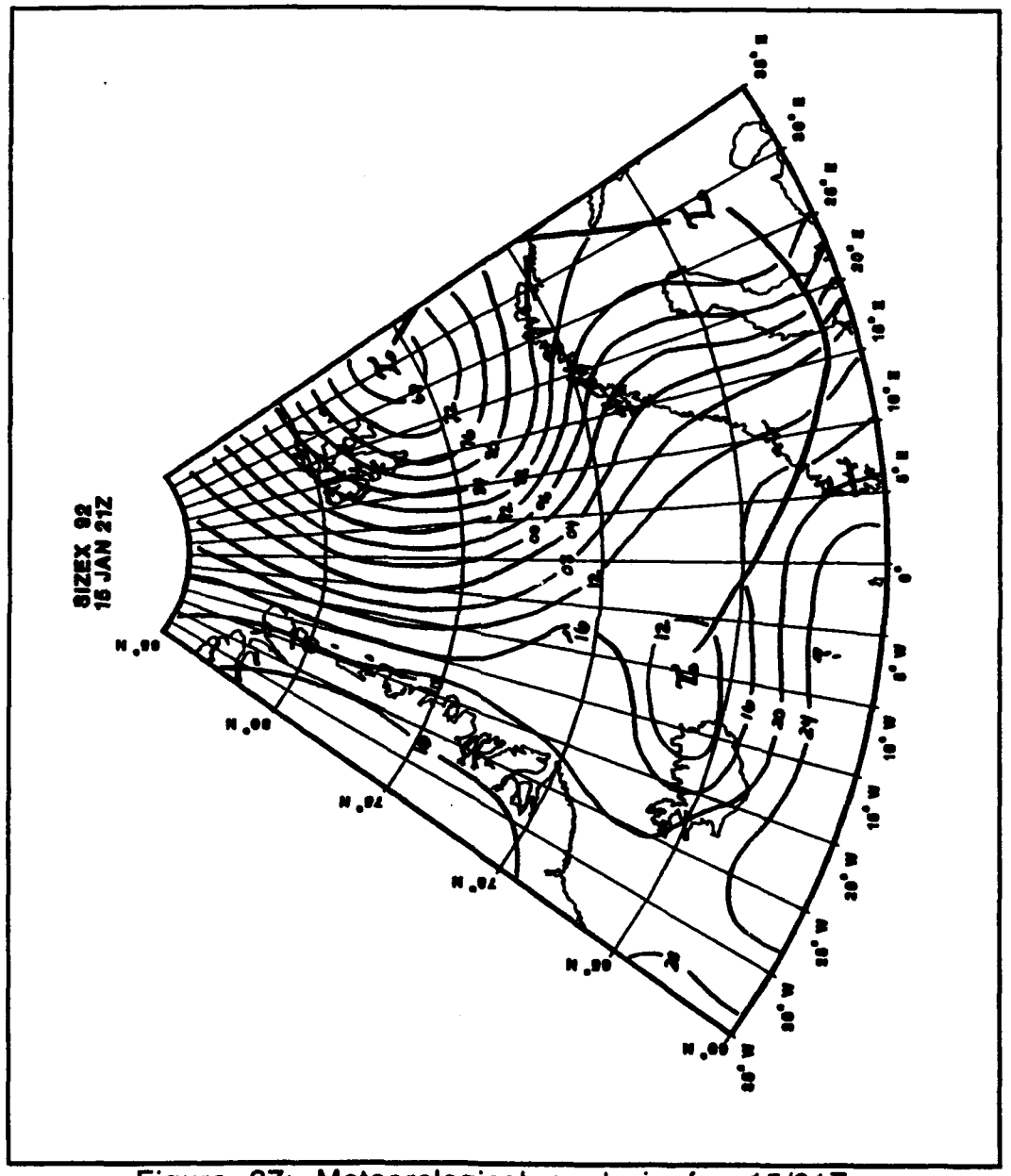

Figure 27: Meteorological analysis for 15/21Z January 1992.

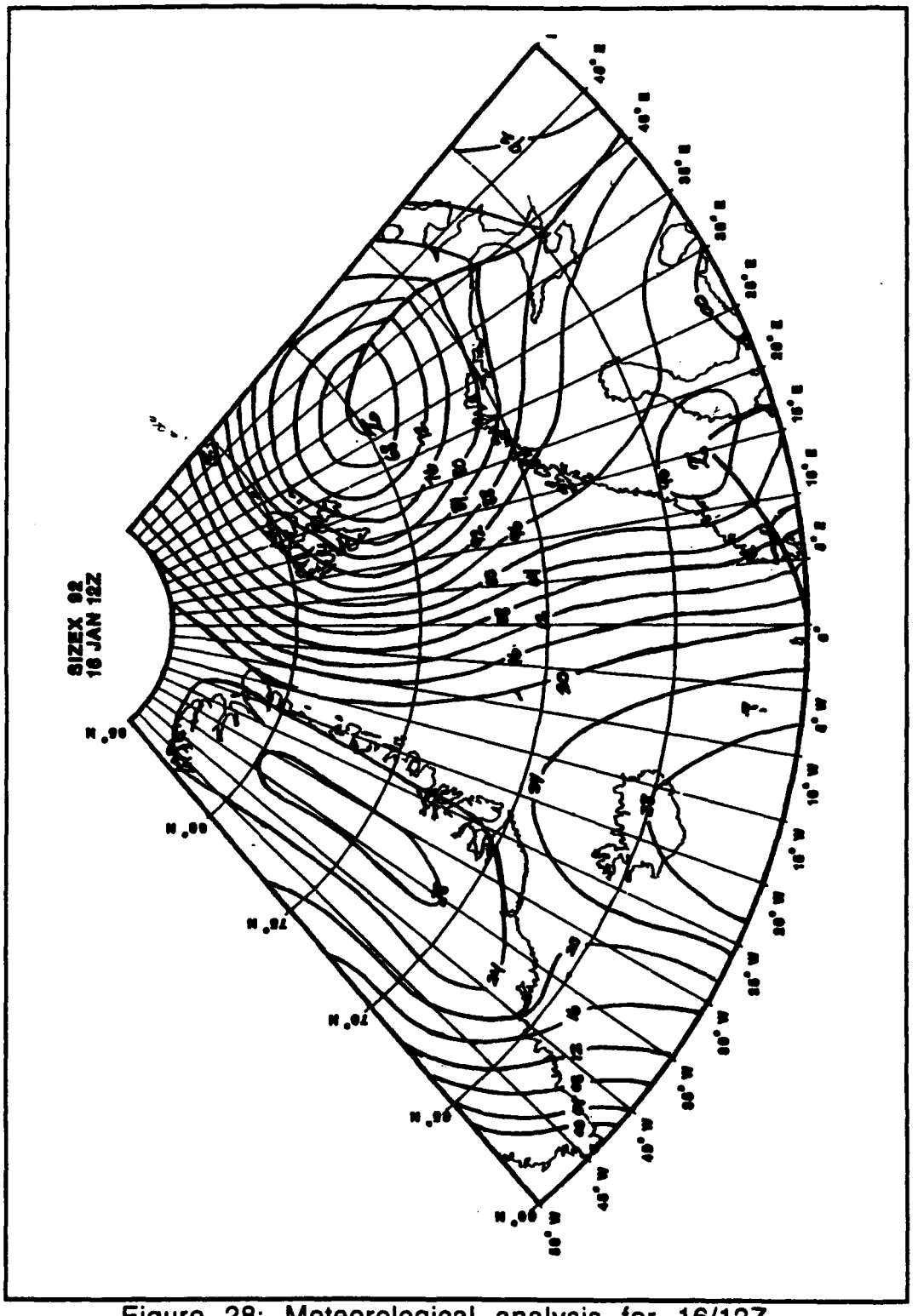

Figure 28: Meteorological analysis for 16/12Z January 1992.

B. MARGINAL ICE ZONE VARIABILITY IN RESPONSE TO WIND FORCING AS INFERRED FROM ERS-1 SAR

Synthetic-aperature radars (SARs) are pulse-doppler radars that transmit short radio pulses to obtain resolution in elevation and use the doppler shift of the backscattered signal to obtain resolution in azimuth. In SAR systems, resolution is independent of distance from the target, unlike optical and real aperature radars where resolution degrades with distance. The power backscattered from the surface is a function of the backscattering coefficient, which is related to the emissivity and penetration depth. The high resolution associated with SAR is the result of the extreme precision with which the doppler shift of the backscattered signal can be determined.

The ERS-1 satellite, equipped with SAR, provided high resolution sequential images of the East Greenland Sea marginal ice zone throughout the SIZEX period. The ground resolution associated with ERS-1 SAR was approximately 25 meters (m). By averaging and reducing speckle noise the imagery resolution became approximately 100 m. The satellite tracks and mean ice edge position are shown in Figure 29. The D4 swath of each satellite pass covered the ice edge between 75°N and 80°N. ERS-1 was placed in a ice orbit with a 3 day exact repeat cycle. The data obtained from each pass was downlinked to the Tromso Satellite Station, processed to full resolution (FRI) and low resolution (LRI), then transmitted to the Nansen Environmental and Remote Sensing Center 2-3 hours after observation in 1000 x 1060 pixels and 16 bit format. The imagery was transformed at NERSC to 1024 x 1024 pixels and 8 bit format, where 1 pixel equalled 20 m. FRI scenes provided approximately 25 m resolution with 3 looks, with a signal to noise ratio of approximately 3:1. LRI scenes provided a much better signal to noise ratio, on the order of 12:1, at the expense of resolution degradation down to 100 m.

SAR has distinct advantages over most other spaceborne sensors in that its effectiveness is not dependent upon meteorological factors. It is capable of "seeing" through the clouds and precipitation that are common along the MIZ. Also, SAR can be used during the dark winter season in high latitudes. When repeated images of the same area are available, detailed descriptions of atmospheric and oceanographic forcing of the ice field can be extracted. For additional information pertaining to the theory of SAR operation, the reader is referred to Shuchman et al. (1991).

Because the SAR responds primarily to spatial variations in surface roughness or backscatter, it is well suited for MIZ studies, where an appreciable change in backscatter can occur over short distances. Surface roughness determines the intensity of radar return by controlling the amount of diffuse backscatter. Backscatter is also dependent on radar wavelength, which interacts with the roughness elements of a reflecting surface. Backscatter from multiyear ice is predominantly due to volume scattering caused by air bubbles, voids and brine pockets. Therefore it has a large number of internal scatterers with dimensions on the order of the radar wavelength. This contrasts with first year ice, which has only a few internal scatterers that are small compared to the radar wavelength. Hence, volume scattering from multiyear ice tends to yield a higher backscatter than the surface scattering which characterizes first year ice. Thus, when interpreting SAR imagery, areas of low signal backscatter appear as dark regions and areas of high signal backscatter appear as bright regions on the image. Caution must be exercised when analyzing SAR imagery, however, because rough surface edges can provide first year ice with high backscatter as well. Similarly, strong wind forcing can produce short surface waves that results in a strong backscatter signal. Nevertheless, preliminary results indicate that ERS-1 SAR demonstrated good capability to distinguish between smooth first

year ice, multiyear ice, grease ice and rubble fields using simple thresholding of backscatter values (Sandven et al., 1992).

In most instances, the ice edge can be described in detail according to its being compact, diffuse, meandering, etc,. Ice edge definition depends upon the contrast between ice and open water signatures in SAR images. The open water signature is heavily dependent upon wind forcing, in that moderate to high winds produce higher backscatter than many ice types observed near the ice edge. Hence, the contrast between ice and open ocean may vary appreciably over time.

SAR imagery has proven useful in the detection and mapping of ocean currents and fronts. As currents interact, the current in the vicinity of a front is modified with respect to the current some distance away, resulting in a straining of small-scale ocean surface waves (Bragg waves) to which SAR is sensitive.

Ice edge non-linearity may be attributed to a combination of dynamic processes which produce deformation. Johannessen et al. (1987) discusses five sources which lead to eddy formation. Likely sources include mixed baroclinic and barotropic instabilities, vortex stretching by interaction with topography and differential Ekman pumping. Ice edge jets are likely caused by baroclinicity associated with the East Greenland Polar Front, the frontal boundary between cold fresh waters of the East Greenland Current and the warmer, more saline Atlantic Intermediate Water seaward of the ice edge (Shuchman et al., 1991).

Thus, in a general sense, the ice edge configuration obtained from SAR imagery provides some insight into the dominant air-ice-ocean forces acting along the MIZ. The ice edge variability during the SIZEX period appeared to be consistent with a SAR conceptual model developed by Johannessen (1993) which was based upon airborne SAR images of the MIZ obtained during previous experiments. This model identifies a relationship between ice edge

configurations and various processes such as: a) upwelling; b) ice-ocean eddies; c) ice jet and vortex pairs; and d) ice banding. The architecture of this model is illustrated in Figure 30.

The morphology of the MIZ exhibited significant variability during the experiment period. The variation in ice edge position and characterization throughout SIZEX can be attributed to both atmospheric and oceanographic forcing. In general, the shape and position of the ice edge was governed by atmospheric forcing with the passage of high latitude low pressure systems, and their associated high wind events. As the wind field relaxed in advance of the next approaching cyclone, upper-ocean dynamics i.e., upper-ocean mesoscale circulations and fronts, were the dominant factor in producing a highly non-linear ice edge. Mesoscale eddies and ice edge jets produced ice tongues which protruded into the open ocean. A description of the ice edge configuration and its variation over the 7-16 January 1992 period follows.

The ice edge on 7 January, Figure 31, appears diffuse and has many mesoscale features. There is a poor delineation between ice and open ocean backscatter near the edge. There appears to be an "Odden" event visible near 74°30'N/8°W, a common feature when off-ice winds are present. This area is characterized by new ice formation (grease ice or nilas, very low backscatter). Odden is the occurrence of nilas 3-5 cm thick ice which transitions into 5-15 cm thick pancake floes 1-3 m in diameter in a particular region. Ice formation occurs off the ice edge where fetch limitation inhibits the growth of fully developed wind waves. Odden is thought to play an important role in deep water formation, as repeated freezing episodes result in sequential density increases. The area of very low backscatter near 74°30'N/8°W is likely due to the formation of new ice which damps the surface Bragg waves.

A 987 mb low pressure system propagated eastward from Iceland to the Norwegian coast during the January 6-7 period. Winds remained predominantly from the northwest in the vicinity of the ice edge at 75°N, due to high pressure over Greenland. The 15 m/s winds evident at 7/12Z in Figure 7 are consistent with HÄKON MOSBY's departure from Tromso, Norway and are probably not present along the MIZ. Instead atmospheric forcing was likely weak-to-moderate over the ice edge from 07/00Z-08/00Z, dominated by high pressure over Greenland. This condition is consistent with the 07/12Z ERS-1 SAR image depicted in Figure 31, in which the ice edge appears very diffuse and difficult to discern.

In the absence of strong atmospheric forcing, the ice edge between 08/00Z and 10/00Z was highly irregular; the result of mesoscale oceanographic forcing. An ascending satellite pass at 08/20Z, shown in Figure 32, clearly shows an oceanic circulation mirrored by grease and pancake ice. This feature is clearly seen in the complex distribution of high and low backscatter at the periphery of the main ice edge near 79°30'N/000°. Numerous ice leads within the ice field are also evident in the image, indicated by dark lines oriented west to east in upper left portion of the image. These observations are consistent with weak westerly winds (1-6 m/s) at the time of the satellite pass. Winds shifted from westerly to southeasterly late in the period as high pressure ridging from the north Atlantic was displaced by an approaching cyclone.

Figure 33 depicts the ice edge configuration at 10/12Z, corresponding to the synoptic time in Figure 16. At the time of the satellite pass, the mesoscale ocean circulation, represented by ice tongues in the imagery, had not been completely masked by ice convergence from on-ice transport. This is perhaps more clearly shown in Figure 34, an ascending SAR image at 10/20Z. Consequently, numerous ice tongues protruding into the open ocean between 76°N and 78°N

are visible in the image. However continued strong northerly flow over the period 10/12Z-11/20Z produced a very compact ice edge, free of any apparent mesoscale oceanic forcing north of 79°N. An ascending satellite pass at 11/20Z, shown in Figure 35, reveals a compact ice edge. A comparison of Figure 32 and Figure 35 clearly shows the effect of the strong atmospheric forcing. The mesoscale circulation near 79°N/000°, mirrored by grease and pancake ice in Figure 32, has disappeared by 11/20Z; presumably collapsed against the ice edge in response to strong northerly flow and Ekman transport. The ice field west of the ice edge has become consolidated. Fewer ice leads and regions of low backscatter are evident when compared to Figure 32. It also appears as though the ice edge has been displaced nearly 30 km to the west.

The compact ice edge evident in Figures 34 and 35 resulted from Ekman forcing by strong easterly and northerly winds. As the deep low pressure center shown in Figure 16 approached and passed to the south, winds at HÄKON MOSBY's position shifted from southerly to easterly over a twelve hour period.

Figure 36 shows the ice edge morpholgy at 13/12Z, approximately three days after the passage of the low pressure system south of HÄKON MOSBY. Mesoscale upper-ocean circulations are clearly mirrored near the ice edge by either pancake ice or small broken floes of multiyear ice. These features are consistent with weak to moderate atmospheric forcing, when ocean forcing plays the dominant role in determining ice edge morphology. The ice edge has also apparently shifted eastward by as much as 40 km in certain regions. A more representative estimate of ice edge displacement is 15-25 km. It is likely that the movement of the ice edge was due to a combination of ice relaxation, as in an elastic medium, mesoscale circulation, and moderate southwesterly winds.

A vortex pair is evident near 77°N/6°W in Figure 36. One plausible mechanism for the development of this feature is a jet normal to the ice edge in

the near-surface layer which developed during the relaxation phase of an upwelling event (Fedorov and Ginsberg, 1986). Strong northerly winds over the 11/00Z-12/06Z period could have created a northerly upper-ocean jet along the ice edge and produced localized upwelling in response to Ekman transport. Ahlnäs et al. (1987) suggests that nonlinear instability is a potential generating mechanism. Strong wind could have produced nonlinear flow and resultant instabilities in the circulation. Unfortunately, neither theory can be verified due to a lack of oceanographic observations.

Also evident in Figure 36 is an ocean frontal feature evident along 79°N. There are clear indications of oceanic circulations in this region, as seen in the backscatter variations in the open ocean. The high backscatter signal evident at the periphery of the ice edge is likely the result of a narrow zone of deformed ice caused by moderate on-ice wind and wave forcing during the several hours prior to the satellite pass.

The onset of another Odden event, in the vicinity of 76°N/6°W, is evident in Figure 36 as well. One possible explanation for the extremely complex circulation pattern evident with the onset of Odden is a localized variation in drag coefficient between new ice and open ocean, superimposed upon a background current (Johannessen, personal communication, 1992).

The SAR image shown in Figure 36 was associated with passage of the cyclone eastward over northern Norway. Figures 17-20 illustrate the progression of this low pressure system. High pressure began ridging over the MIZ, resulting in a dramatic decrease in wind speed and an abrupt shift to southwesterly winds, as recorded in Figure 7. In response to the weak-to-moderate atmospheric forcing over the period 12/00Z-13/00Z the ice edge "relaxed" and shifted eastward. Late in this period, another low pressure system had tracked along the

coast of Greenland and entered the Greenland Sea, causing a easterly wind shift.

Figures 37 and 38 show the ice edge configuration at 14/20Z and 16/12Z, respectively. The passage of an intense low pressure system was the dominant mechanism forcing the ice edge morphology after 13/12Z. Ice leads seen in Figure 35 (11/20Z) are no longer clearly apparent in Figure 37 due to ice advection into the region. Mesoscale ocean circulation evident in Figure 36 has been completely masked by the strong northwesterly wind. The Odden event which was evident on the 13 January image is no longer visible by 16 Janaury. The high wind and wave activity that occurred over this period disintegrated the new ice and masked any mesoscale ocean circulation in its vicinity. Any complex eddy activity has disappeared as the pancake ice which served as a tracer was consolidated into the ice edge or disintegrated by wave action. The ocean front seen in the 13 January image along 79°N is no longer visible by 16 January. This is not to say that the frontal signature has been erased by strong northwesterly flow--simply that the higher backscatter of wave acitivity precludes its detection.

Despite strong winds during the period preceeding the satellite pass, there appears to be indications of mesoscale ocean circulation near 77°N/6°W, evidenced by an ice tongue which protrudes from the ice edge at this position. The persistence of this feature may be attributable to the effects of topographic steering of the East Greenland Current as it follows the curving shelf break in this region (Johannessen, personal communication, 1992).

Ice bands or streamers are clearly visible in the 16 January SAR image, Figure 38. The occurrence of ice bands is a phenomenon frequently observed in the marginal ice zones. There are several proposed theories pertaining to the formation of such structures. Wadhams (1983) suggests that the wave radiation

pressure of a fetch-limited sea produced by off-ice winds blowing over water openings is responsible for these features. Häkkinen (1986) maintains that a temporally varying wind field, and the associated upwelling/downwelling responses associated with Ekman transport, create variations in the pycnocline--inducing band formation. Chu (1987) proposes that in the presence of a strong ice-to-open-water temperature gradient a mesoscale feedback mechanism generates zones of ice convergence and divergence, hence ice banding. Each of these theories is consistent with the northwesterly (off-ice) wind observed over the 15-16 January period. In the case of Häkkinen (1986), pycnocline variability could have occurred between 12-16 January, when the wind field shifted 180°. It is indeed unfortunate that oceanographic observations were not available to confirm the various model predictions.

Figure 39, an ascending SAR image at 16/20Z, shows the result of the persistent off-ice winds over the 14-16 January period. The interior of the ice edge appears diffuse, with numerous leads (lines of low backscatter) again evident in the imagery.

The high winds that occurred over the three day period preceeding Figures 38 and 39 were associated with the development of an intense low pressure system over the Greenland Sea. This system tracked eastward and, by 13/12Z, had reached HÄKON MOSBY's position. It deepened substantially over the next 24 hours, producing strong northerly winds. Figures 21-28 illustrate the progression of this cyclone.

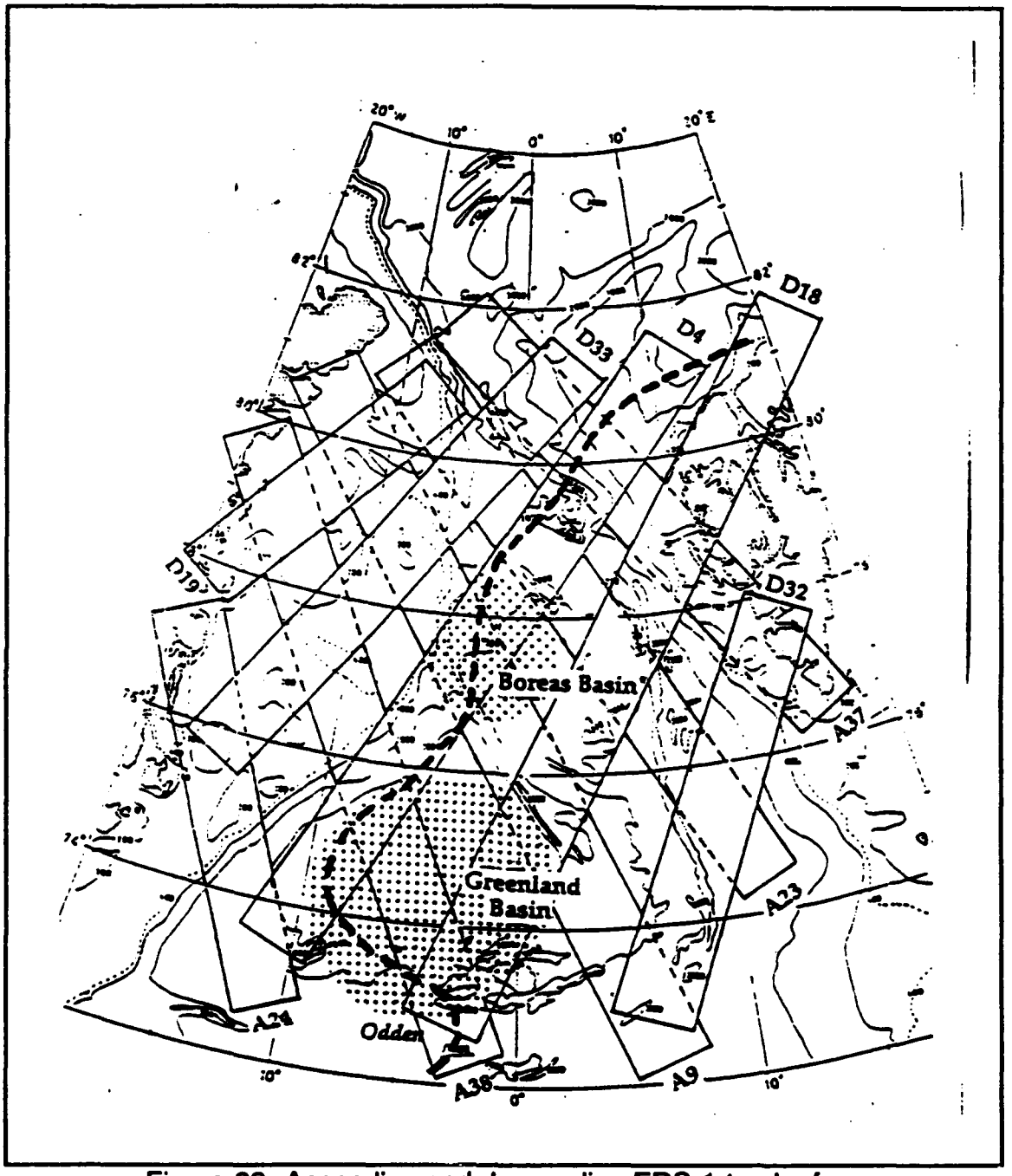

Figure 29: Ascending and descending ERS-1 tracks for SIZEX '92. Mean ice edge position is indicated by a dashed line (from O.M. Johannessen, NERSC Technical Report).

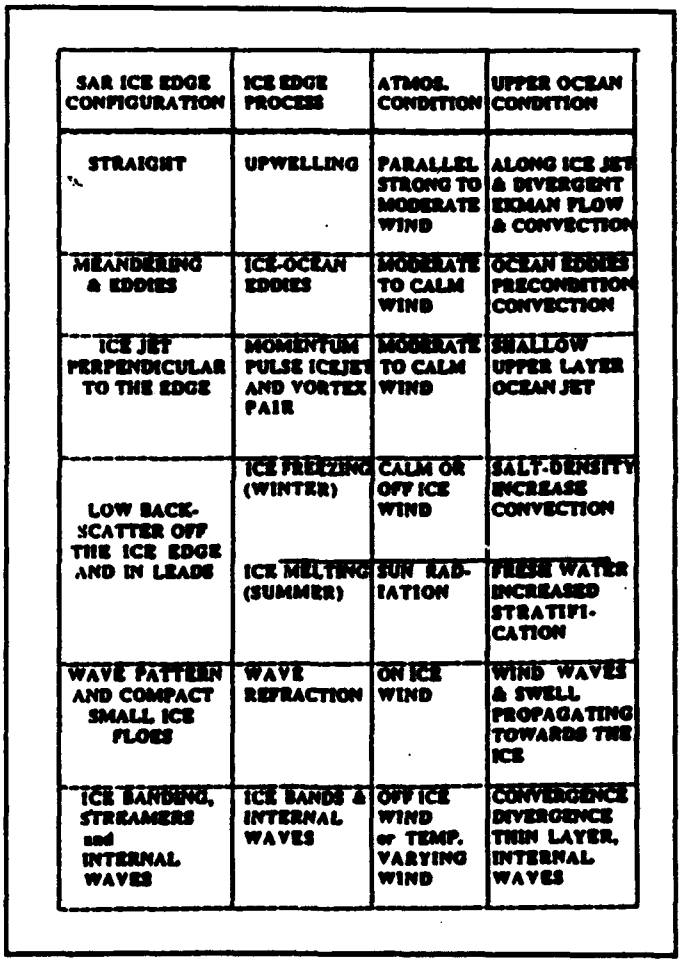

SAR ICE EDGE CONFIGURATION	ICE EDGE PROCESS	ATMOS. CONDITION	UPPER OCEAN CONDITION
STRAIGHT	UPWELLING	PARALLEL STRONG TO MODERATE WIND	ALONG ICE JET & DIVERGENT EKMAN FLOW & CONVECTION
MEANDERING & EDDIES	ICE-OCEAN EDDIES	MODERATE TO CALM WIND	OCEAN EDDIES PRECONDITION CONVECTION
ICE JET PERPENDICULAR TO THE EDGE	MOMENTUM PULSE ICEJET AND VORTEX PAIR	MODERATE TO CALM WIND	SHALLOW UPPER LAYER OCEAN JET
LOW BACK-SCATTER OFF THE ICE EDGE AND IN LEADS	ICE FREEZING (WINTER)	CALM OR OFF ICE WIND	SALT-DENSITY INCREASE CONVECTION
	ICE MELTING (SUMMER)	SUN RADIATION	FRESH WATER INCREASED STRATIFICATION
WAVE PATTERN AND COMPACT SMALL ICE FLOES	WAVE REFRACTION	ON ICE WIND	WIND WAVES & SWELL PROPAGATING TOWARDS THE ICE
ICE BANDING, STREAMERS and INTERNAL WAVES	ICE BANDS & INTERNAL WAVES	OFF ICE WIND or TEMP. VARYING WIND	CONVERGENCE DIVERGENCE THIN LAYER, INTERNAL WAVES

Figure 30: SAR conceptual model (from Johannessen, 1993)

Figure 31: ERS-1 SAR image for 07/12Z Jan 1992 (from Johannessen et al., 1993)

Figure 32: ERS-1 SAR image for 08/20Z Jan 1992 (from Johannessen et al., 1993)

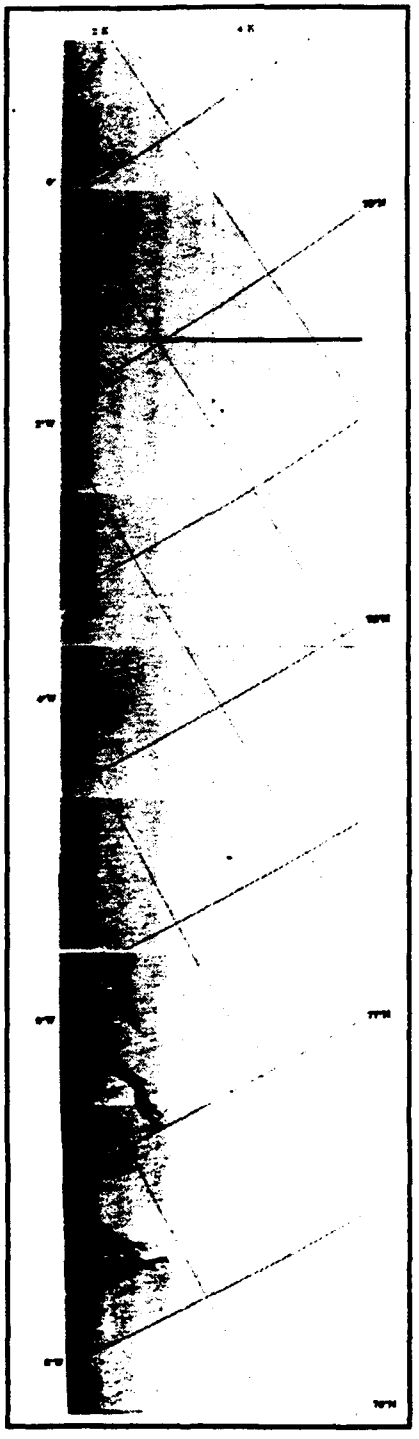

Figure 33: ERS-1 SAR image for 10/12Z Jan 1992 (from Johannessen et al., 1993)

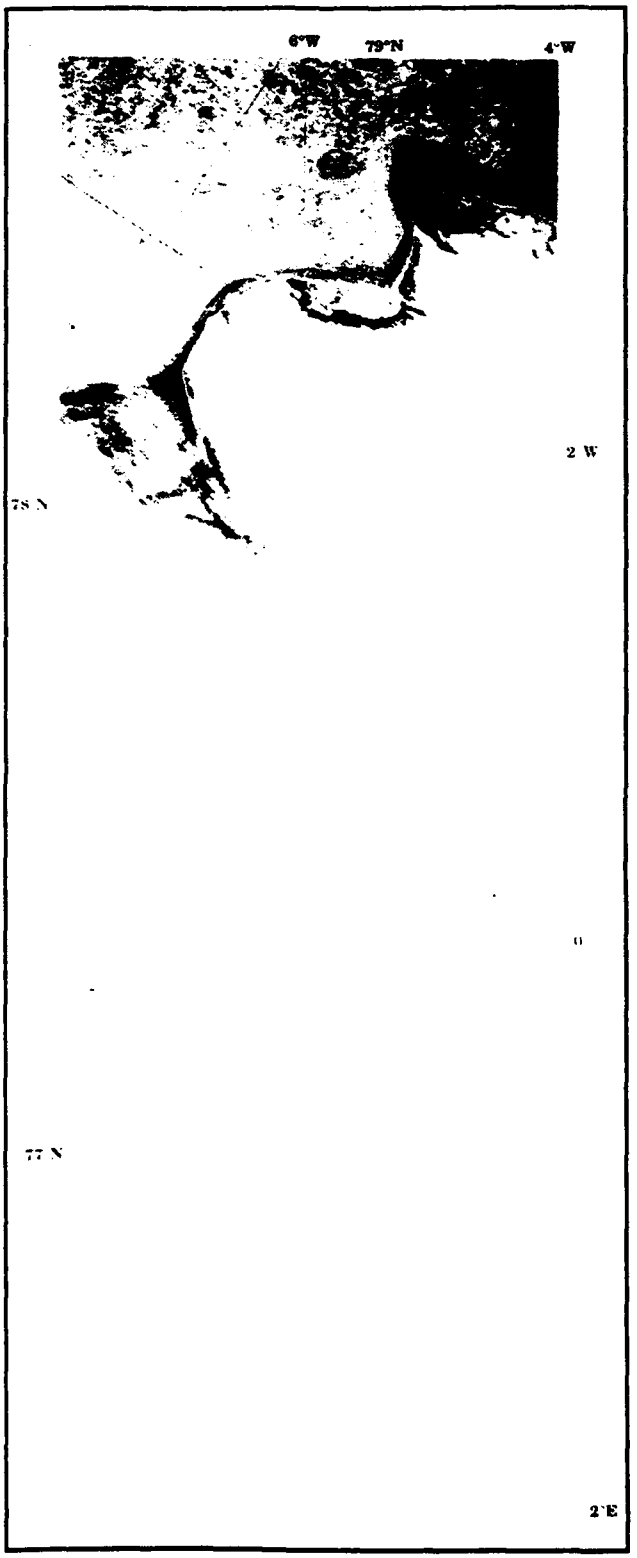

Figure 34: ERS-1 SAR image for 10/20Z Jan 1992 (from Johannessen et al., 1993)

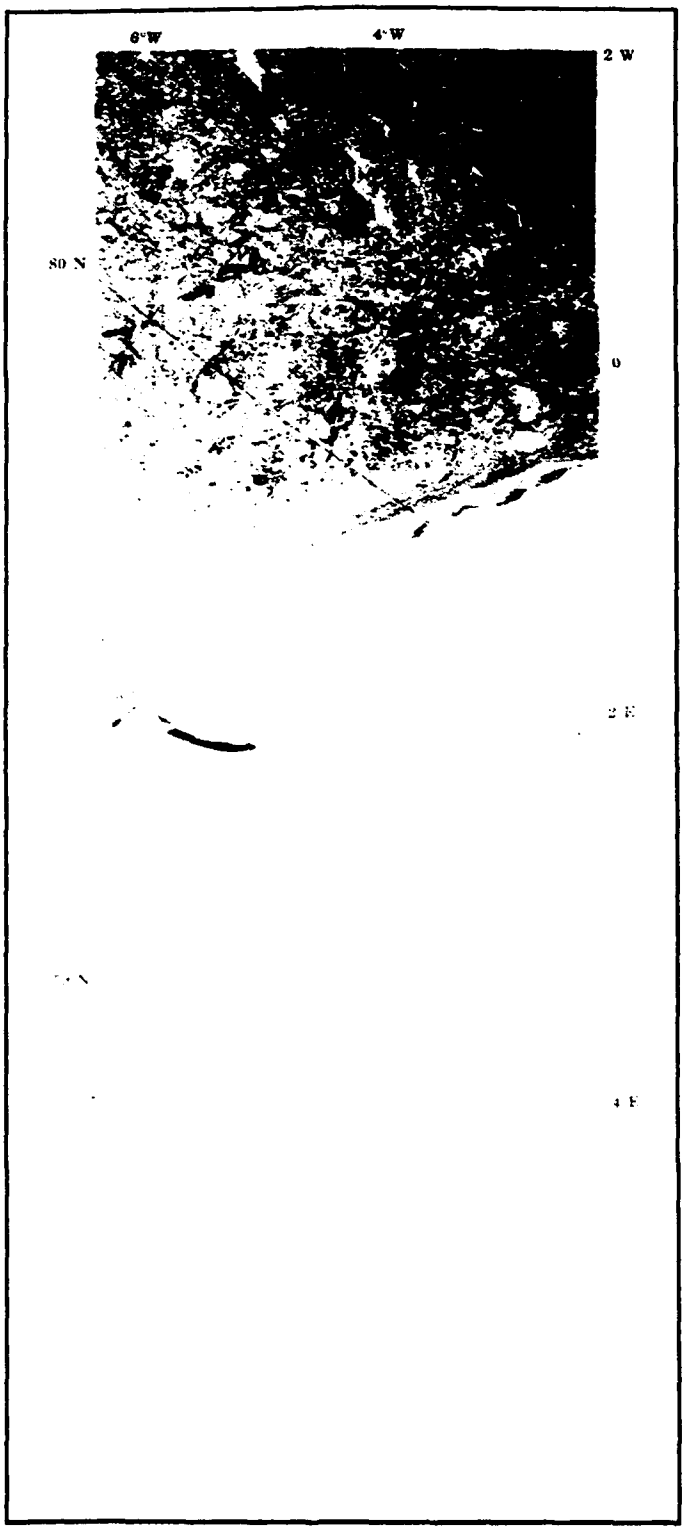

Figure 35: ERS-1 SAR image for 11/20Z Jan 1992 (from Johannessen et al., 1993)

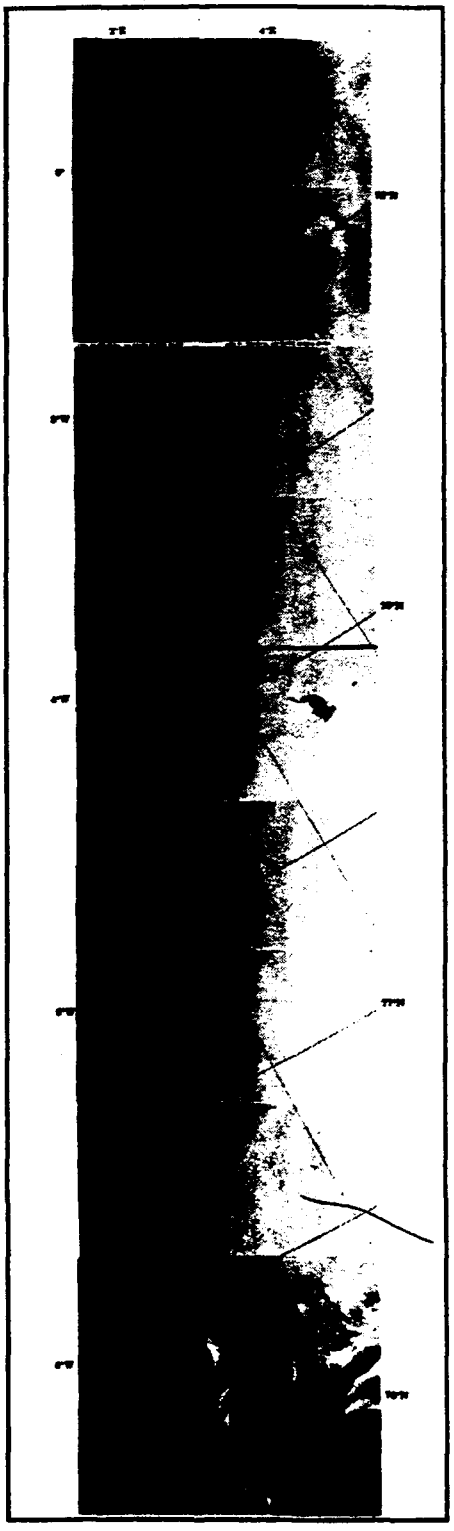

Figure 36: ERS-1 SAR image for 13/12Z Jan 1992 (from Johannessen et al., 1993)

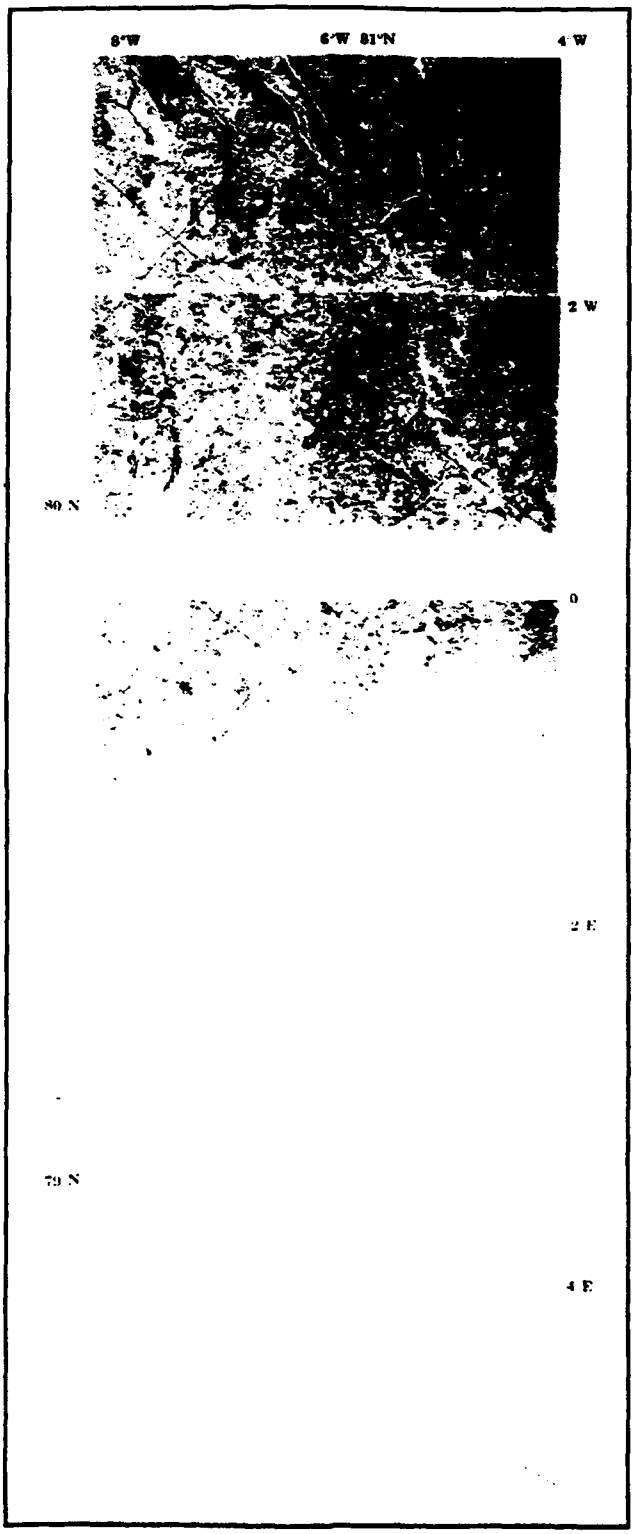

Figure 37: ERS-1 SAR image for 14/20Z Jan 1992 (from Johannessen et al., 1993)

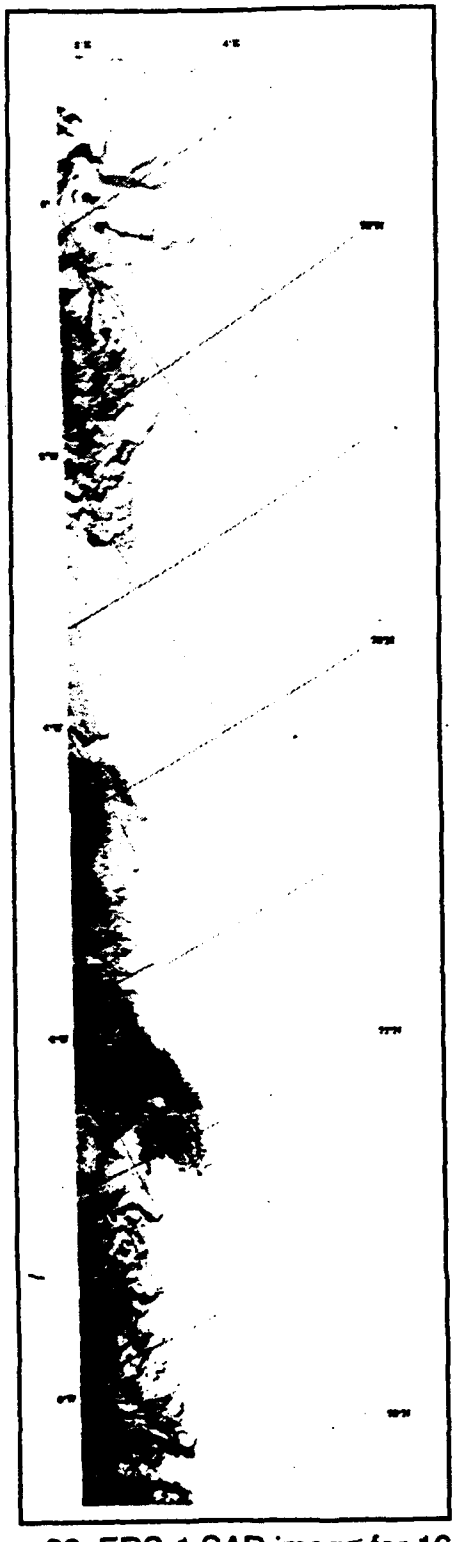

Figure 38: ERS-1 SAR image for 16/12Z Jan 1992 (from Johannessen et al., 1993)

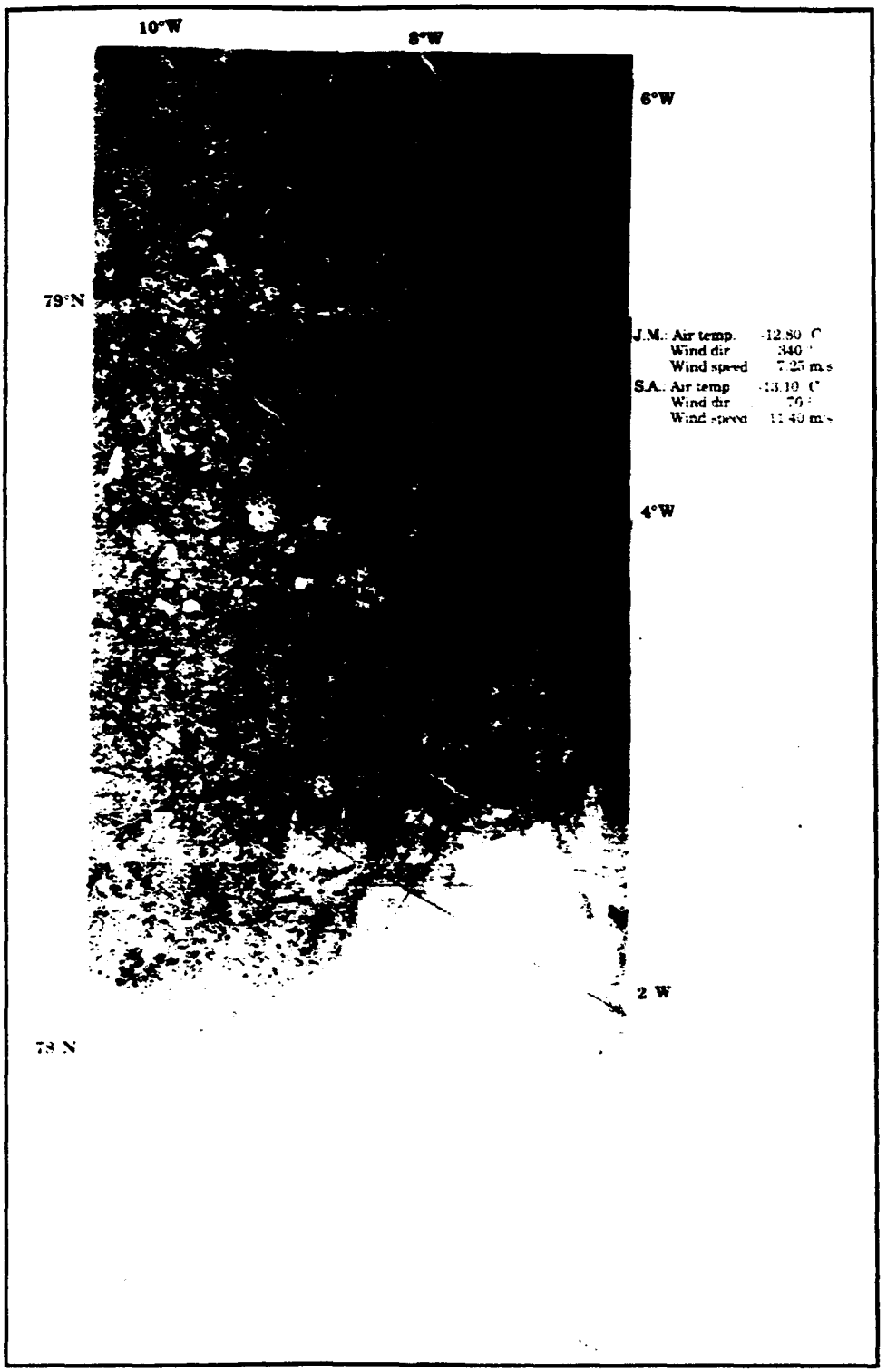

Figure 39: ERS-1 SAR image for 16/20Z Jan 1992 (from Johannessen et al., 1993)

C. SAR VERSUS SSM/I-DETERMINED ICE EDGE POSITION

An accurate determination of the ice edge position is important for both military and commercial applications. The U.S. Navy's submarine fleet routinely operates beneath the polar ice cover. Hence, knowledge of ice edge position, ice thickness distribution, keel depths, etc., is essential for personnel safety and mission success. Similarly, commercial shipping uses ice edge position and concentration to plan transit routes. Nations which rely on the polar oceans as a resource have long-recognized the high biologic productivity and abundance of petroleum in these regions, and routinely use ice concentration and ice edge position data.

While SAR is the most accurate and efficient means of delineating the ice edge, it may not be possible to view the ice edge daily. Other operational sensors must be used to infer the position of the ice edge, despite an uncertainty associated with the degraded resolution.

Campbell et al. (1987) and Svendsen et al. (1983) compared SMMR-derived ice concentrations with high resolution observations. These studies formed the basis for a comparison of ice edge position determined from SAR and SSM/I. Their comparison of aircraft microwave, visual observations and SMMR ice concentration distribution plots indicated that for the summer MIZ the 30% SMMR ice concentration isopleth correlated best with actual diffuse ice edge positions. Similarly, the compact ice edge correlated best with the 40-50% ice concentration isopleth. Observations acquired during the Norwegian Remote Sensing Experiment (Svendsen et al., 1983) indicated that in the Greenland Sea for the fall-winter period the actual ice edge position correlated best with the 50% SMMR ice concentration isopleth.

A redefinition of the ice edge is required before contrasting the SAR-derived ice edge position with SSM/I ice concentration isopleths. Campbell et al. (1987)

and Svendsen et al. (1983) considered the ice edge to be the outer limits of small, packed floes. Such features are generally not visible in the SAR D4 swath during the SIZEX period. Instead, they are found to the west of these images. Therefore, to facilitate the comparison, the ice edge in the SAR imagery is defined as the outer limit of minimum backscatter, i.e., seaward extent of new ice. However, the reader is cautioned that only a rough comparison of the two sensors can be made due to the large difference in scale. The SSM/I will tend to smooth the ice edge, due to its poor resolution, and will not detect mesoscale ice edge features.

The SAR-derived ice edge position was compared with SSM/I ice concentration to determine whether the relationship between ice edge classification (compact, diffuse) and ice concentration isopleth remained valid for the a) SSM/I sensor; b) in winter months; and c) a redefined ice edge.

SSM/I ice concentration isopleths were obtained for 10, 13, 16 and 19 January. The 30% and 50% ice concentration isopleths were compared to the ice edge position determined from SAR imagery at approximately the same observation times. The comparisons are illustrated in Figures 40-43.

The SSM/I 30% and 50% ice concentration isopleths for 10 January are shown in Figure 40, with the rightmost line indicating the 30% isopleth. The ice concentration gradient is very pronounced, a characteristic which is consistent with a compact ice edge produced by strong on-ice winds. The undulations evident in the isopleths may at first yield a conflicting conclusion to Campbell et al. (1987), however it is likely that the duration of on-ice winds wasn't sufficient to smooth large scale protuberances. When the ice edge determined from Figure 33 is compared to the SSM/I 30% and 50% isopleths it becomes apparent that the SAR-derived ice edge is in rough agreement with the 50% isopleth. One notable exception in Figure 38 is the region between 76°30'N and 77°N, where

the ice edge closely corresponds to the 30% isopleth. Here the ocean circulation is advecting new ice into open ocean. This region was interpreted by the SSM/I algorithm to be mostly open water. Similarly, SSM/I viewed the ice tongues between 77°N and 78°N as mostly open water.

On 13 January the meteorological condition (Figure 22) and corresponding SAR image (Figure 36) suggest a period of weak atmospheric forcing and a diffuse ice edge. This situation is mirrored in the relaxed ice concentration gradient depicted in Figure 41. The ice edge inferred from the SAR imagery is also included in Figure 41. The ice edge is generally in close agreement (within 10 km) with the 30% ice concentration isopleth, consistent with the findings of Campbell et al. (1987). While individual filaments and ice tongues are not resolved by SSM/I, the gross nature of the ice edge is well-represented.

The ice edge position and SSM/I ice concentration isopleths for 16 January are shown in Figure 42. The synoptic meteorological situation (Figure 28) indicates a period of strong off-ice winds. The gross position of the ice edge north of 77°N corresponds to a 40% ice concentration isopleth. However, south of 77°N the ice edge position is poorly approximated by the 30% or 50% ice concentration isopleths. In certain areas the error in ice edge position is estimated to exceed 25 km. The reason for the inadequacy of the SSM/I algorithm south of 77°N is unclear. It is possible that a spatial variation in the wind field produced a more diffuse ice edge to the south. This, in conjunction with the large SSM/I footprint, may have led to such an error.

Finally, the 19 January SAR ice edge and ice concentration isopleths are shown in Figure 43. Atmospheric forcing was again weak and the ice field appears to have relaxed. The SSM/I ice concentration gradient diminished over the 16-19 January period, indicative of a more diffuse ice edge. The ice edge appears to be well-represented by the 30% isopleth in most areas. The two

notable exceptions are the ice edge north of 78°30′N and the edge in the vicinity of 76°30′N.

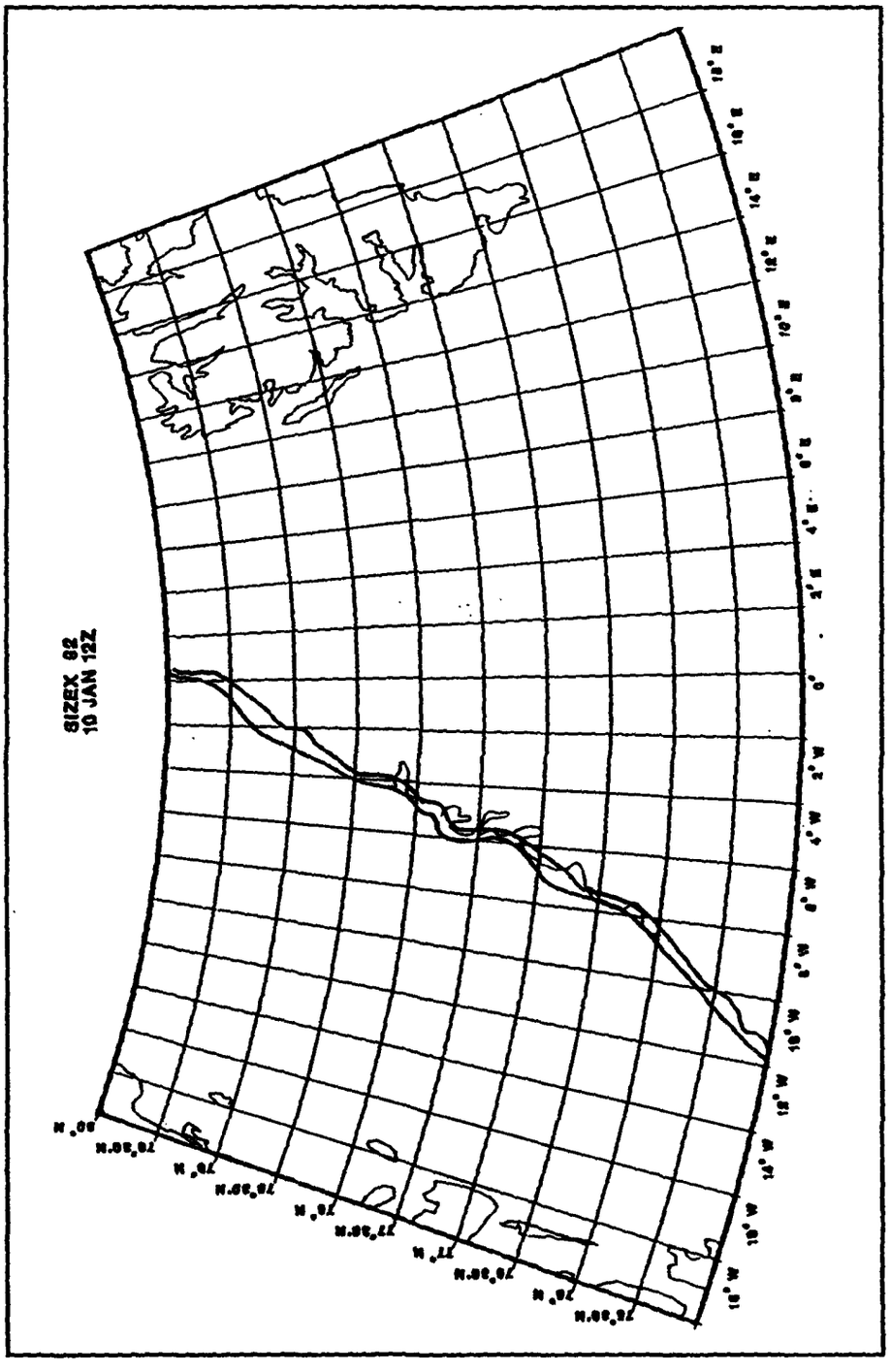

Figure 40: SSM/I vs. SAR-inferred ice edge for 10 Jan 1992. Bold lines represent 50% (left) and 30% (right) isopleths. Plain line represents SAR ice edge.

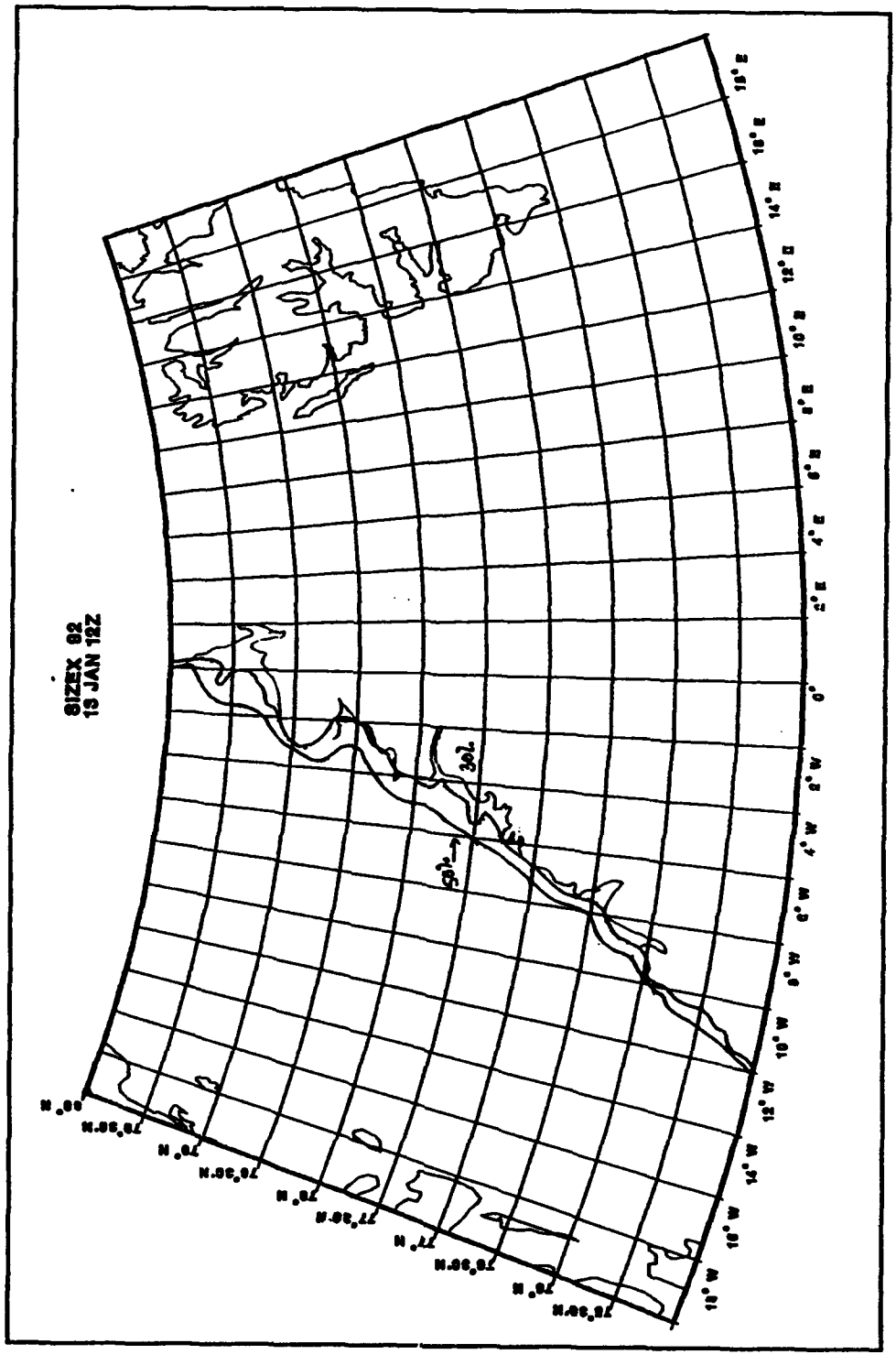

Figure 41: SSM/I vs. SAR-inferred ice edge for 13 Jan 1992. Bold lines represent 50% (left) and 30% (right) isopleths. Plain line represents SAR ice edge.

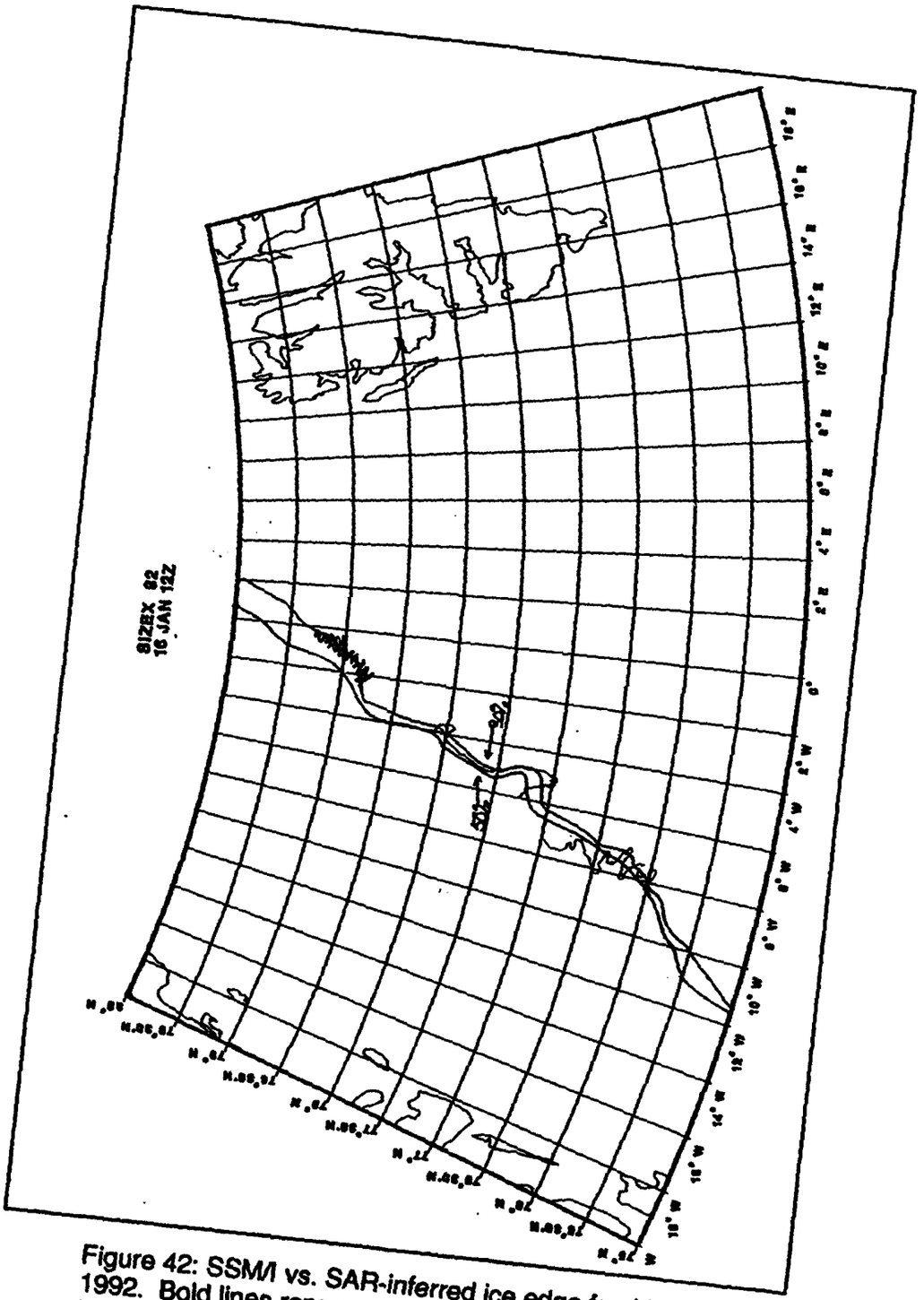

Figure 42: SSM/I vs. SAR-inferred ice edge for 16 Jan 1992. Bold lines represent 50% (left) and 30% (right) isopleths. Plain line represents SAR ice edge.

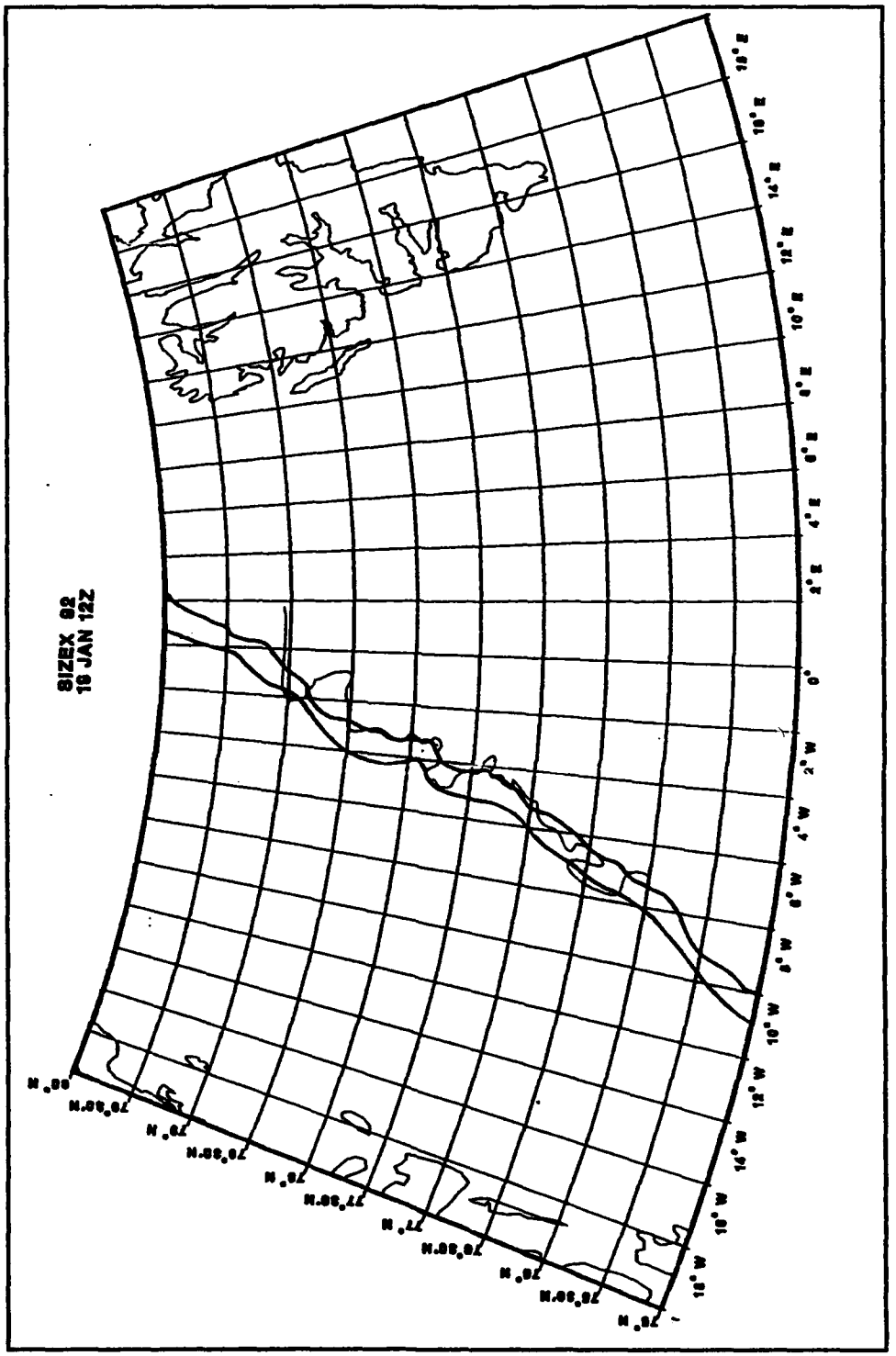

Figure 43: SSM/I vs. SAR-inferred ice edge for 19 Jan 1992. Bold lines represent 50% (left) and 30% (right) isopleths. Plain line represents SAR ice edge.

III. SUMMARY AND RECOMMENDATIONS

A. SUMMARY

The marginal ice zone is composed of first year ice, broken-up multiyear floes, and a variety of new ice types. Ice within several kilometers of the ice edge can be subjected to wave induced breakup as swell propagates into the ice and places a stress on the floes. Ice in close proximity to open ocean is often deformed by numerous collisions. The end result of this deformation can be a large neutral drag coefficient for ice within the marginal ice zone. Thus, the ice edge responds dynamically to variations in wind stress imposed by high pressure ridging and arctic low pressure systems which cross the Greenland Sea.

High latitude cyclones often form off the coast of Newfoundland in response to strong baroclinicity associated with the polar front or circumpolar vortex. In the winter months, when the horizontal temperature gradient and surface heat fluxes are particularly pronounced, very intense low pressure systems may form and propagate into the Greenland Sea. These systems generally follow the baroclinic zones or waves, manifested in low-level and mid-level steering flows.

During the Seasonal Ice Zone Experiment in January 1992, the marginal ice zone was subjected to two high wind speed events between 10-16 January. The changes observed in marginal ice zone morphology were recorded in the form of spatial and temporal backscatter variations by the ERS-1 synthetic-aperature radar. In response to the strong easterly and northerly flow associated with the passage of these cyclones to the south, the ice edge became compact and assumed a relatively linear configuration. Persistent off-ice winds produced banding along the ice edge. There is also evidence that the fringes of the ice edge respond very quickly, on the order of a few hours, to spatial and temporal

variations in the wind field. Mesoscale ocean circulations, manifested by spatial variations in backscatter or by ice floes acting as effective tracers, were generally dominated by atmospheric forcing in such instances. The mesoscale features were not visible on SAR imagery, either because the high ocean backscatter (from wind waves) masked any ocean signature or because the ice floes disintegrated or were consolidated into the ice edge.

When atmospheric forcing diminished after the passage of a low pressure system, the ice edge was displaced 15 to 25 kilometers towards the east. It is likely that this movement was a combination of an elastic-like response to the relaxation of internal stress upon the ice and weak-to-moderate off-ice winds as high pressure ridged into the region. With atmospheric forcing no longer dominant, mesoscale circulations became an important process in altering the ice edge morphology. The ice edge configuration appeared highly non-linear, with numerous ice tongues, bights and fronts evident in the SAR imagery. Hence, atmospheric and oceanic forcing act to produce a cyclical change in the marginal ice zone morphology by alternately compressing and expanding the ice edge. These observations were consistent with a SAR conceptual model which was developed to account for these various ice edge features.

By defining the ice edge determined from SAR to be the outer limit of minimum backscatter, the SAR-inferred ice edge could be related to SSM/I ice concentration isopleths. When the ice edge was compared with 30% and 50% isopleths, a compact ice edge produced by atmospheric forcing loosely corresponded to a 50% isopleth. If the ice edge was characterized as diffuse, it was well-represented by the 30% isopleth. As expected, the passive SSM/I isopleths could not identify detailed ice edge features evident in the SAR imagery. These features were considered to be mostly open water with concentrations less than 30%. These results do not necessarily contrast with

conclusions drawn by Svendsen et al. (1983) since the ice edge is defined differently.

B. RECOMMENDATIONS

A spaceborne SAR sensor in a three day exact repeat orbit is capable of detecting ice edge variations in response to the passage of storms. However, the three day data gap is unsatisfactory for determining significant storm-caused variations along the ice edge. These are of the order of 1 day or less. Additionally, in many instances the three day data gap is unacceptable for the study of ice kinematics. During prolonged period of high wind stress, it is likely the object being studied will be advected outside the image swath, thus making estimations of velocity impossible. In order to improve our understanding of ice kinematics and the short-term MIZ response to arctic cyclones it will be necessary to either utilize multiple high resolution sensors or place the SAR in a more frequent exact repeat orbit.

It is readily apparent that atmospheric forcing can produce significant changes in ice edge morphology. However, it is also obvious that ocean circulation plays an equally important role. To better understand and quantify the role of oceanographic features in modifying ice edge morphology, it is necessary to collect and analyze both meteorological and oceanographic observations at various positions along the ice edge. Thus it would be possible to:

-- determine the extent to which ocean circulation opposes or contributes to wind forcing in changing ice edge morphology

-- determine whether oceanographic features were masked from SAR imagery or interrupted by high wind events

-- determine if spatial variations in the wind field produce a different ice edge morphology

-- quantify and explain the various oceanic circulations near the ice edge evident in SAR imagery, i.e., vortex pairs, jets, eddies.

-- identify recurrent regions of Odden events and analyze the density structure of the water column underlying the recent ice formation

LIST OF REFERENCES

Aagaard, K., "The Wind-Driven Transports in the Greenland and Norwegian Seas", *Deep Sea Res.*, vol. 17, 281-291 (1970).

Ahlnäs, K., T.C. Royer and T.H. George, "Multiple Dipole Eddies in the Alaska Coastal Current Detected With Landsat Thematic Mapper Data", *J. Geophys. Res.*, vol. 92, no. C12, 13041-13047 (1987).

Barry, R.G., "Aspects of the Meteorology of Sea Ice", in *The Geophysics of Sea Ice*, ed. by Norbert Untersteiner, Plenum Press, NY, 993-1020 (1986).

Burns, B.A., and G. Kellner, "Correlation of SAR-Derived Roughness Parameters With Air Drag Coefficients Over MIZ Sea Ice", *Preprints-Second Conference on Polar Meteorology and Oceanography*, American Meteorological Society, Boston, 75-78 (1988).

Campbell, W.J., P. Gloersen, E.G. Josberger, O.M. Johannessen, P.S. Guest, N. Mognard, R. Shuchman, B.A. Burns, N. Lannelongue, and K.L. Davidson, "Variations of Mesoscale and Large-Scale Sea Ice Morphology in the 1984 Marginal Ice Zone Experiment as Observed by Microwave Remote Sensing", *J. Geophys. Res.*, vol. 92, no. C7, 6805-6824 (1987).

Carleton, A.M., "Synoptic Sea Ice-Atmosphere Interactions in the Chukchi and Beaufort Seas From Nimbus 5 ESMR Data", *J. Geophys. Res.*, vol. 89, no. D5, 7245-7258 (1984)

Chu, P.C., "An Instability Theory of Ice-Air Interaction for the Formation of Ice Edge Bands", *J. Geophys. Res.*, vol. 92, no. C7, 6966-6970 (1987).

Federov, K.N. and A.I. Ginsburg, "Mushroom-like Currents (vortex dipoles) In The Ocean and In A Laboratory Tank", *Annales Geophysicae*, vol. 4, no. B5, 507-516 (1986).

Guest, P.S. and K.L. Davidson, "The Effect of Observed Ice Conditions on the Drag Coefficient in the Summer East Greenland Sea Marginal Ice Zone", *J. Geophys. Res.*, vol. 92, 6943-6954 (1987).

Häkkinen, S., "Ice Banding as a Response of the Coupled Ice-Ocean System to Temporally Varying Winds", *J. Geophys. Res.*, vol. 91, no. C4, 5047-5053 (1986).

Johannessen, O.M., W.D. Hibler III, P. Wadhams, W.J. Campbell, K. Hasselmann, and I. Dyer, "Marginal Ice Zones: A Description of Air-Ice-Ocean Interactive Processes, Models and Planned Experiments", *Arctic Technology and Policy*, ed. by I. Dyer and C. Chryssostomidis, Hemisphere Publishing Corporation, NY, 122-146 (1984).

Johannessen, O.M., "Brief Overview of the Physical Oceanography", in *The Nordic Seas*, edited by B.G. Hurdle, Springer Verlag, NY, 103-127 (1986).

Johannessen, J.A., O.M. Johannessen, E. Svendsen, R. Shuchman, T. Manley, W.J. Campbell, E.G. Josberger, S. Sandven, J.C. Gascard, T. Olaussen, K. Davidson, and J. Van Leer, "Mesoscale Eddies in the Fram Strait Marginal Ice Zone During the 1983 and 1984 Marginal Ice Zone Experiment", *J. Geophys. Res.*, vol. 92, 6754-6772 (1987).

Johannessen, J.A., Personal Communication with the Author, Nansen Environmental and Remote Sensing Center, Solheimsvik, Norway, January (1992)

Johannessen, O.M., S. Sandven, and K. Kloster, NERSC *Technical Report*, in press, Nansen Environmental and Remote Sensing Center, Solheimsvik, Norway (1993).

Johannessen, O.M., "Microwave Remote Sensing of Sea Ice", in *ONR/NASA Scientific Monograph*, ed. by R. Carsey, in press (1993).

Johnson, C.M., "Wintertime Arctic Ice Extremes and the Simultaneous Atmospheric Circulation", *Mon. Wea. Rev.*, vol. 108, 1782-1791 (1980).

LeDrew, E.F., "The Role of Local Heat Sources in Synoptic Activity Within the Polar Basin", *Atmosphere-Ocean*, vol. 22(3), 309-327 (1984).

Mosby, H., "Water, Salt and Heat Balance of the North Polar Sea and of the Norwegian Sea", *Geofysiske Publikasjoner*, vol. 24, 1-66 (1962).

Overland, J.E., "Atmospheric Boundary Layer Structure and Drag Coefficients Over Sea Ice", *J. Geophys. Res.*, vol. 90, no. C5, 9029-9049 (1985).

Overland, J.E., and K.L. Davidson, "Geostrophic Drag Coefficients Over Sea Ice", *Tellus*, vol. 44A, 54-66 (1992).

Perry, R.K., "Bathymetry", in *The Nordic Seas*, edited by B. Hurdle, Springer-Verlag, NY (1986).

Sandven, S., O.M. Johannessen and K. Kloster, NERSC *Technical Report no.* 65, Nansen Environmental and Remote Sensing Center, Solheimsvik, Norway, 14 pp. (1992).

Sater, J.E., A.G. Ronhovde, and L.C. van Allen, *Arctic Environment and Resources*, Arctic Institute for North America, Washington, DC, 310 pp (1971).

Sechrist, F.S., R.W. Fett and D.C. Perryman, *Forecasters Handbook for the Arctic*, T.R. 89-12, Naval Environmental Prediction Research Facility, Monterey, CA, 364 pp. (1989).

Serreze, M.C. and R.G. Barry, "Synoptic Activity in the Arctic Basin, 1979-85", *J. Climate*, vol. 1, 1276-1295 (1988).

Shuchman, R.A., B.A. Burns, O.M. Johannessen, E.G. Josberger, W.J. Campbell, T.O. Manley, and N. Lannelongue, "Remote Sensing of the Fram Strait Marginal Ice Zone, *Science*, vol. 236, 429-431 (1987).

Shuchman, R.A., C.C. Wackerman and L.L. Sutherland (Eds.), *"The Use of Synthetic Aperature Radar To Map the Polar Oceans - A Remote Sensing Manual"*, Environmental Research Institute of Michigan, Ann Arbor, MI, 328 pp. (1991).

Svendsen, E., K. Kloster, B. Farrelly, O.M. Johannessen, J.A. Johannessen, W.J. Campbell, P. Gloersen, D. Cavalieri, and C. Matzler, "Norwegian Remote Sensing Experiment: Evaluation of the Nimbus 7 Scanning Multichannel Microwave Radiometer for Sea Ice Research", *J. Geophys. Res.*, vol. 88, 2781-2791 (1983).

Thorndike, A.S., and R. Colony, "Sea Ice Motion in Response to Geostrophic Winds", *J. Geophys. Res.*, vol. 87, 5845-5852 (1982).

Trengeled, S., "Oceanography of the Norwegian and Greenland Seas and Adjacent Areas, Volume II--Survey of 1870-1970 Literature", *Saclant ASW Res. Centre Memorandum SM-47,* Italy (1974).

Wadhams, P., "The Seasonal Ice Zone", in *The Geophysics of Sea Ice*, ed. by Norbert Untersteiner, Plenum Press, NY, 825-922 (1986).

Wadhams, P., "A Mechanism for the Formation of Ice Edge Bands", *J. Geophys. Res.*, vol. 88, no. C5, 2813-2818 (1983).

Worthington, L.V., "The Norwegian Sea as a Mediterranean Basin", *Deep Sea Res.*, vol. 17, 77-84 (1970).

INITIAL DISTRIBUTION LIST

		No. Copies
1.	Defense Technical Information Center Cameron Station Alexandria, VA 22304-6145	2
2	Library, Code 52 Naval Postgraduate School Monterey, CA 93943-5002	2
3.	Chairman (Code MR/Hy) Department of Meteorology Naval Postgraduate School Monterey, CA 93943-5000	1
4.	Professor Kenneth L. Davidson (Code MR/Ds) Department of Meteorology Naval Postgraduate School Monterey, CA 93943-5000	2
5.	Dr. Peter S. Guest (Code MR/Gs) Department of Meteorology Naval Postgraduate School Monterey, CA 93943-5000	2
6.	LT Steven J. Rutherford, USN Naval Polar Oceanography Center, Suitland Washington, DC 20373	1
7.	Commander Naval Oceanography Command Stennis Space Center, MS 39529-5000	1
8.	Comanding Officer Naval Oceanographic and Atmospheric Research Laboratory Stennis Space Center, MS 39529-5004	1
9.	Chief of Naval Research 800 North Quincy Street Arlington, VA 22217	1

No. Copies

10. Superintendent 1
Naval Research Laboratory
NPS Annex, Code 7500
Monterey, CA 93943-5006

11. Dr. Stephen F. Ackley 1
Department of Oceanography
Naval Postgraduate School
Monterey, CA 93943-5000